Functional and phenotypic differences of pure populations of stem cell-derived astrocytes and neuronal precursor cells

Journal:	*GLIA*
Manuscript ID	GLIA-00248-2015.R2
Wiley - Manuscript type:	Original Research Article
Date Submitted by the Author:	19-Nov-2015
Complete List of Authors:	Kleiderman, Susanne; University of Konstanz, Biology Sa, Joao; IBET/ITQB, TCA Lab Teixeira, Ana; IBET/ITQB, TCA Lab Brito, Catarina; IBET/ITQB, TCA Lab Gutbier, Simon; University of Konstanz, Chair of in-vitro Toxicology and Biomedicine/Alternatives to Animal Experimentation Evje, Lars; Norwegian University of Science and Technology, Department of Neuroscience Hadera, Mussie; Norwegian U of Science & Tech, Neuroscience Glaab, Enrico; Université du Luxembourg, Luxembourg Centre for Systems Biomedicine Henry, Margit; University of Cologne, Center of Molecular Medicine Agapios, Sachinidis; University of Cologne, Center of Molecular Medicine Alves, Paula; IBET/ITQB, TCA Lab Sonnewald, Ursula; Norwegian U of Science & Tech, Neuroscience Leist, Marcel; University of Konstanz, Biology
Key Words:	astrocytes, neural stem cells, differentiation, metabolic flux, transcriptome

Functional and phenotypic differences of pure populations of stem cell-derived astrocytes and neuronal precursor cells

Susanne Kleiderman[1], João V. Sá[2], Ana P. Teixeira[2], Catarina Brito[2], Simon Gutbier[1], Lars G. Evje[3], Mussie G. Hadera[3], Enrico Glaab[4], Margit Henry[5], Sachinidis Agapios[5], Paula M. Alves[2], Ursula Sonnewald[3], and Marcel Leist[1].

[1]: The Doerenkamp-Zbinden Chair of in-vitro Toxicology and Biomedicine/Alternatives to Animal Experimentation, University of Konstanz, Konstanz, Germany,

[2] : IBET - Instituto de Tecnologia Química e Biológica, Universidade Nova de Lisboa, Av. da República, 2780-157 Oeiras, Portugal,

[3]: Department of Neuroscience, Faculty of Medicine, Norwegian University of Science and Technology, NO-7491 Trondheim, Norway,

[4]: Luxembourg Centre for Systems Biomedicine, University of Luxembourg, L-4366 Belvaux, Luxembourg,

[5]: Institute of Neurophysiology and Center for Molecular Medicine Cologne (CMMC), University of Cologne, 50931 Cologne, Germany.

Running title: functional distinction of NSC and astrocytes

Number of words: Abstract 249; Introduction 751; Materials and Methods 2023; Results 4610; Figure legends 2222; Discussion 2241; Bibliography 2539; Acknowledgements 55; Figures: 9; Tables: 0; Supplementary figures: 18, supplementary tables: 0; total word count: 14,692

Send correspondence to:

Susanne Kleiderman née Kirner
University of Konstanz
PO Box M657
D-78457 Konstanz
Germany
Susanne.Kirner@uni-konstanz.de
Tel.: +49-7531-885136
Fax: +49-7531-885039

Main Points:

- Rapid generation of a homogeneous population of mature, non-dividing astrocytes
- Comparison of embryonic stem cell-derived astrocytes (mAGES) and neural stem cells (NSC)
- Differences of NSC and mAGES concerning function, metabolism, and transcriptome

Keywords: astrocytes, neural stem cells, differentiation, metabolic flux, transcriptome.

Acknowledgements:

This work was supported by a grant of the DFG-funded graduate school RTG 1331 (S.K.), the KoRS-CB (M.L.), and the Doerenkamp-Zbinden foundation. JVS is the recipient of a PhD fellowship (PD/BD/52474/2014) from FCT Portugal,

Embryonic stem cell lines BTBR T^{+} *Itpr3*^{tf} /J-PB60.6 and DO335.45 were kindly provided by Predictive Biology, Inc., Carlsbad, CA, USA.

Abstract

Availability of homogeneous astrocyte populations would facilitate research concerning cell plasticity (metabolic and transcriptional adaptations; innate immune responses) and cell cycle reactivation. Current protocols to prepare astrocyte cultures differ in their final content of immature precursor cells, pre-activated cells or entirely different cell types. A new method taking care of all these issues would improve research on astrocyte functions. We found here that the exposure of a defined population of pluripotent stem cell-derived neural stem cells (NSC) to BMP4 results in pure, non-proliferating astrocyte cultures within 24-48 h. These murine astrocytes generated from embryonic stem cells (mAGES) expressed the positive markers GFAP, aquaporin 4 and GLT-1, supported neuronal function, and acquired innate immune functions such as the response to TNF and IL-1. The protocol was applicable to several normal or disease-prone pluripotent cell lines, and the corresponding mAGES all exited the cell cycle and lost most of their nestin expression, in contrast to astrocytes generated by serum-addition or obtained as primary cultures. Comparative gene expression analysis of mAGES and NSC allowed quantification of differences between the two cell types and a definition of an improved maker set to define astrocytes. Inclusion of several published data sets in this transcriptome comparison revealed the similarity of mAGES with cortical astrocytes *in vivo*. Metabolic analysis of homogeneous NSC and astrocyte populations revealed distinct neurochemical features: both cell types synthesized glutamine and citrate, but only mature astrocytes released these metabolites. Thus, the homogeneous cultures allowed an improved definition of NSC and astrocyte features.

Introduction

The definition of astrocyte functions and developmental potential, in particular in relation to neural stem cells, is still a dynamic area of research (Bayraktar et al., 2015; Gotz et al., 2015; Robel et al., 2011). Astrocytes and neural stem cells (NSC) share several phenotypic and functional features (Doetsch et al., 1999; Kriegstein and Alvarez-Buylla, 2009; Levitt and Rakic, 1980; Seri et al., 2001). Moreover, some types of NSC (radial glia or astrocytes from the subventricular zone) have been categorized as members of the heterogeneous group of astrocytes, due to their expression of the glial fibrillary acidic protein (GFAP), the most frequently used astrocyte marker (Eng et al., 2000; Ihrie and Alvarez-Buylla, 2008; Steindler and Laywell, 2003). Under pathophysiological conditions, astrocyte behavior shows high plasticity (Parpura et al., 2012) and reversion to an NSC-like precursor state has been observed (Gotz et al., 2015; Sirko et al., 2013).

Astrocytes play a pivotal role in brain metabolism (Amaral et al., 2011; McKenna et al., 2012; Waagepetersen et al., 2009) and in linking neurons and other brain cells to blood supply (Kacem et al., 1998). Beside their role in metabolic homeostasis, astrocytes efficiently take up neurotransmitters like glutamate (Zhou and Danbolt, 2013), and thus modulate synaptic function (Perea et al., 2009). In this context, glial glutamine synthetase (Glul) catalyzes the condensation of ammonia to imported glutamate to produce glutamine, which is then released, and taken up by neurons to produce glutamate again (Daikhin and Yudkoff, 2000). This dynamic recycling mechanism of glutamate, considered essential to prevent neuronal excitotoxicity (Delaney et al., 1996), is thought to be astrocyte-specific. However, NSC also express the glutamate-aspartate transporter GLAST (Liu et al., 2006; Ullensvang et al., 1997) and glutamine synthetase (Hernández et al., 1999; Monzon-Mayor et al., 1990; Suarez et al., 1997) and their potential role in glutamate metabolism therefore deserves attention.

For the study of astrocyte metabolism and function, primary monolayer cultures have become the dominating model system. However, contamination with other cell types such as microglia (Saura, 2007), requires stringent controls and the contribution of immature cells with high levels of nestin expression to standard primary cultures has often been neglected (Hansson, 1986; Sergent-Tanguy et al., 2006; Stahlberg et al., 2011). An alternative approach to obtain astrocytes is to use neurospheres from embryonic stem cells (ESC) (Kuegler et al., 2012) or brain (Crocker et al., 2008) as starting material for astrocytogenesis. The resulting astrocyte population is free of microglia, but it may still contain nestin-positive precursors and various proliferating cell types. The same applies to the generation of human astrocytes from pluripotent stem cells. Several corresponding protocols generate GFAP-positive cells

(Krencik et al., 2011; Roybon et al., 2013; Shaltouki et al., 2013), but they all still contain sizable subpopulations of immature or contaminating cells that might spoil results of gene expression analysis, identification of metabolic pathways, or cell fate examinations.

Compared to astrocytes, hardly any data is available on metabolism or inflammatory reactions of their precursor cells and of NSC. A major reason for this paucity of information may be the limited access to suitable experimental systems. Isolation of defined and sufficiently large populations of primary cells is difficult, and NSC amplified *in vitro* in the form of neurospheres often comprise heterogeneous subpopulations that are challenging to handle for biochemical studies.

A new option to study NSC was provided by the discovery that such cells may be cultured and propagated as highly homogeneous monolayer cultures (Conti et al., 2005). This seminal work mainly described the use of the cells to study neurogenesis, but it was also shown that this NSC cell population differentiated to GFAP-positive cells within 48 h of exposure to serum (Conti et al., 2005). These data suggested an attractive way of producing astrocytes (Schneider, 2014; Schneider and d'Adda di Fagagna, 2012; Sparmann et al., 2013), but more characterization of the resultant cells is necessary, and the original protocol requires adaptations and further specifications before pure cultures of astrocytes can be obtained reproducibly.

Since there is a great, yet largely unrecognized, potential in the astrocyte generation from NSC, we set out to i) define the critical steps of the procedure, ii) to characterize the resulting cells, and iii) to demonstrate the usefulness of a protocol adapted from Conti et al. 2005 for generating NSC and astrocyte populations. This allowed us for the first time a direct comparison of NSC and homogeneous, non-proliferating astrocytes concerning differentiation response, neuronal support, immune activation, differentially-expressed genes, and metabolic features with clear differences identified between the two cell types.

Materials and Methods

Maintenance of murine embryonic stem cells (mESC)

The mESC lines CGR8.0, E14, BTBR T+ Itpr3tf/J-PB60.6 (The Jackson Laboratory, 002282C01), DO335.45 (Diversity Outbred strain, Jax number 009376), and O9 iPS (Wernig et al., 2007) were maintained in Glasgow Minimum Essential Medium (GMEM) containing high glucose (4.5 g/l), 10% fetal bovine serum (FBS), 2 mM Glutamax, 2 mM sodium pyruvate, 2 mM non-essential amino acids, and 50 µM β-mercaptoethanol (materials are listed in the supplementary). Medium was changed every day with freshly added 1,000 U/ml leukemia inhibitory factor (LIF). Cells were passaged every other day with 0.05% trypsin and replated on Nunclon^{TM} Delta flasks (Thermo Scientific) coated for 1 h with 0.1% gelatin dissolved in water.

Differentiation of neural stem cells from mESC

Cultures of mESC were used when they reached 80% confluency. Cells were harvested with 0.05% trypsin, pelleted and replated as single cells in 'N2B27-medium' [1 part DMEM/F12 + 1 part Neurobasal-medium, supplemented with N2 and B27, 2 mM Glutamax, 100 µM β-mercaptoethanol, 7.5 µg/ml insulin, 50 µg/ml bovine serum albumin (BSA)] at a density of 10,000 cells/cm^2 on 10 cm Nunclon dishes coated for 2 h with 0.1% gelatin. Medium was changed every other day. On day 7, cells were treated with 0.05% trypsin for 1 min, resuspended with N2B27-medium and filtered through a 70 µm cell strainer into 50 ml polypropylene tubes prefilled with phosphate buffered saline (PBS) to dilute trypsin. After centrifugation at 500 x g for 3 min, all cells were plated onto gelatin-coated T75 Nunclon flasks in N2B27-medium supplemented with 20 ng/ml FGF2 and 20 ng/ml EGF. For cryopreservation, cells were trypsinized and cryopreserved in FBS containing 10% DMSO at 2×10^6 cells/ml.

Maintenance and selection of NSC from freshly prepared d7NSC

After the 7 days neural induction of mESC, cells were grown in N2B27 medium supplemented with EGF and FGF2. The cells in these initial cultures had different morphologies and cell cycling behavior, some of them growing faster than others. Since the desired bipolar, RC2-positive NSC can be rare at passage 1, cultures were not passaged until they reached full confluency (~ 1 week). To get rid of aggregating cells, which sit on top of other cells, plates were tapped several times to detach them mechanically before trypsinization. Some aggregating cells are usually in closer contact with other cells as well as the coated surface; therefore they cannot be removed by tapping the flasks. They were

manually scratched with an aspiration pipette (aggregates are visible with the naked eye) and the borders of the flask were scratched as well. To separate bipolar NSC from triangular flat cells, cultures were treated with trypsin for only 10-15s. Under these conditions, NSC detach in contrast to the more adherent triangular cells. Pictures before and after mechanical cleaning and selective trypsinization are shown in the supplemental figure S2. After trypsinization, the flask surface was washed only once with N2B27 medium to harvest bipolar NSC and avoid detaching triangular cells. The harvested cells were thoroughly resuspended in one corner of the flask to obtain single cells. Since NSC are very sensitive to trypsin, the cell suspension was directly diluted in about 20 ml PBS (through 70 µm cell strainer), centrifuged rapidly afterwards, and resuspended in medium. After several passages, the aggregating and the triangular cells disappeared. At about passage 8-12, cultures purely consisted of bipolar NSC. Sometimes aggregating cells reappeared after passage 8, but they were easily removed as described above. Notably, NSC do not tend to aggregate when passaged twice a week at the right density. They should not be seeded at less than 10,000 cells per cm^2 and should be passaged at maximum 90% confluency (70-80% confluency is better). For maintenance culture, flasks with at least 75 cm^2 should be used, since NSC tended to clump in smaller flasks.

Astrocyte differentiation

NSC cultures from passage 8 or later at 80% confluency were treated with 0.05% trypsin for 10-15 seconds, resuspended in N2B27-medium and filtered through a 70 µm cell strainer prefilled with PBS, centrifuged (500 x g, 3 min), and resuspended in medium. Cells were plated at a density of 30,000 (e.g. for NFkB translocation) to 50,000 (e.g. for metabolic studies) cells/cm^2 in N2B27-medium supplemented with 20 ng/ml bone morphogenetic protein 4 (BMP4). Nunclon dishes or plates were coated with 10 µg/ml poly-L-ornithine-hydrobromide in PBS for 2 h at 37°C, washed twice with PBS, and coated with 2 µg/ml laminin in PBS overnight. Laminin was aspirated and the cell suspension was added to dishes/plates. Medium was changed every other day from day 1 and experiments were performed at day 3 or 5 of differentiation. If cells were cultured for longer periods, medium was changed every other day using N2B27-medium with 10 ng/ml BMP4.

Preparation and maintenance of primary astrocytes

BALB/c mice were bred at the animal facility of the University of Konstanz (Konstanz, Germany). All mice were housed at 22°C and 55% relative humidity in a 12-h day/night rhythm with free access to food and water according to national regulations and EU guideline

2010/63/EU. Primary astrocytes were prepared from 1-2 days old mouse pups as described earlier (Henn et al., 2011). Briefly, cells were pre-purified by a percoll density gradient centrifugation right after dissociation of the cortices. The enriched astrocyte fraction was kept in tissue culture flasks for two weeks in medium containing 20% FBS. Then, they were trypsinized and plated for experiments.

Quantitative RT-PCR

Total RNA was isolated using PeqGold TriFast (Peqlab, Erlangen, Germany) according to the manufacturer's instructions and 1 µg of RNA was reverse transcribed to cDNA using the iScript RT PCR Supermix kit (Biorad). Quantitative-RT-PCR (qPCR) to measure mRNA expression levels was performed using a CFX96^{TM} Real Time System (BioRad, Hercules, CA) and SSO Fast EvaGreen Supermix (Biorad) according to the manufacturer's protocol. The cDNA levels relative to the housekeeping gene *Gapdh* were calculated using the delta C_T method. Primers used are listed in supplemental material.

Immunofluorescence staining and EdU labeling

Cells were fixed for 10 min with ice-cold 90% methanol at -20°C, permeabilized with 0.1% Triton X-100 in PBS at RT for 10 min, and blocked for 30 min in 1% BSA in PBS. Cells were stained with primary antibodies for 2 h and the respective secondary antibodies (Invitrogen, Darmstadt, Germany) for 50 min. 1 µg/ml H-33342 was added during the last 20 min to counterstain DNA. Primary antibodies used are listed in the supplementary. To detect DNA synthesis, cells were incubated for 48 h with the thymidine analogue EdU (Baseclick, BCK-EdU555), fixed and permeabilized as described above, and stained according to manufacturer's instruction.

Microarray profiling and data analysis

RNA of 4 independent cultures and differentiations of mESC, NSC, and 5-days old mAGES was isolated from 3 pooled technical replicates as described for qPCR. Microarray analysis was conducted as described earlier (Krug et al., 2013). Briefly, 12.5 µg fragmented aRNA was hybridized with Affymetrix Mouse Genome 430 2.0 arrays according to the manufacturer's instructions. All reagents and instruments were acquired from Affymetrix (Affymetrix, Santa Clara, CA, USA). The generated CEL files were used for further statistical analysis. All microarray datasets were pre-processed using the GC-RMA procedure for background correction, quantile normalization and probe replicate summarization (Wu et al., 2004). All statistical analyses were performed in the R Statistical Programming Environment (Ihaka and Gentleman, 1996). Differentially expressed genes between pairs of conditions

were determined using the Empirical Bayes moderated t-statistic (Smyth, 2004) and adjusted for multiple hypothesis testing using the Benjamini-Hochberg method (Benjamini and Hochberg, 1995). A false-discovery rate threshold of 0.05 was chosen to determine the significantly differential genes.

Protein measurement and LDH release

Cells were lysed in 2% sodium dodecyl sulfate (SDS) and protein content of lysates was measured using Pierce™ BCA Protein Assay Kit (Thermo Scientific) according to the manufacturer's protocol. For the release of lactate dehydrogenase (LDH), 10 µl (one-tenth of total volume) of supernatant and cell lysates (20 min 0.1% Triton-X100) were used together with 200 µl reaction mix containing 1:50 pyruvate to NADH reagent (68 µg/ml pyruvate in KPP buffer [40.24 mM K_2HPO_4, 9.7 mM KH_2PO_4, pH 7.5] and 8.47 mg/ml NADH in 1% $NaHCO_3$). NADH oxidation was measured at 340 nm with BioTek EL808 Absorbance Reader for 20 min. LDH release in percent was calculated from ΔOD_{340} (supernatant)/(ΔOD_{340} (supernatant) + ΔOD_{340} (lysate)).

Glutamate uptake measurement

Cells were pre-incubated with Hanks' Balanced Salt Solution (HBSS, Gibco) containing 1 g/l glucose. After 30 min, 10 µM L-glutamic acid (G1624, Sigma) was added supplemented with 0.12 µCi L-[3,4-^{3}H]-glutamic acid (PerkinElmer, NET490250UC) per sample. After 8 min, cells were washed 4 times with HBSS and lysed with 0.5% Triton-X100 for 30 min. Lysates were mixed 1:1 with Ultima Gold AB scintillation cocktail (PerkinElmer, G013309) and measured with the LS 6500 scintillation counter (Beckman Coulter).

Culture condition for metabolic flux analysis and metabolite extraction

NSC and mAGES were seeded in 6 well plates in their normal condition. NSC were maintained 2 days until they were about 60% confluent and mAGES were differentiated until day 5. Cells were washed twice with pre-warmed PBS and incubated in N2B27-medium without glucose [1:1 Neurobasal-A and Advanced DMEM/F-12] supplemented with 10 mM D-[1-^{13}C]-glucose-for 0, 0.3, 3, 12, and 24 h. Medium was collected, centrifuged at 200 g for 10 min, and supernatant was frozen at -20°C until further processing. Cells were washed twice with ice-cold PBS, frozen in liquid nitrogen, and extracted with 70% ethanol. After centrifugation of the cell extracts for 15 min at 20,000 g, supernatants were collected and stored at -80°C until further analysis. Pellets were stored at -20°C for protein determination.

Measurement of glucose, lactate, and amino acids in supernatant

Glucose and lactate concentrations in samples of cell supernatants were determined using an automated YSI 7100 Multiparameter Bioanalytical System (Dayton, OH, USA). Extracellular concentrations of amino acids were quantified by HPLC using a pre-column derivatization method based on the Waters AccQ Tag Amino Acid Analysis method as described elsewhere (Amaral et al., 2010).

Quantification of mass isotopomers by GC-MS

Analysis of ^{13}C percent enrichment in metabolites was carried out by redissolving lyophilized extracts in 0.01M HCl. Samples were extracted in multiple steps into an organic phase of ethanol and benzene and lyophilized before derivatization with N-Methyl-N-(t-Butyldimethylsilyl)trifluoroacetamide + 1% t-butyldimethylchlorosilane (MTBSTFA). The samples were analyzed on an Agilent 6890 gas chromatograph (GC) connected to an Agilent 5975B mass spectrometer (MS) (Agilent Technologies, Palo Alto, CA, USA). The parent ion (M) and atom percent excess for one, two, n ^{13}C atom (M+1,2, n) values for metabolites were calculated from GC-MS data using MassHunter software supplied by Agilent (Agilent Technologies, Palo Alto, CA, USA) and corrected for the naturally abundant ^{13}C by using non-enriched standards (Walls et al., 2014).

1H-NMR spectroscopy for citrate determination in cell culture supernatants

Citrate concentration in samples of cell supernatants was determined by 1H-NMR spectroscopy, in a 500MHz Avance spectrometer (Bruker, Billerica, MA) with a 5 mm QXI probe. Spectra were recorded at 25º C, using a NOESY-based pulse sequence with water presaturation, performing 256 scans, with 4 s acquisition time and 2 s relaxation delay. DSS-d6 (Sigma Aldrich, St. Louis, MO; USA) was used as internal standard. Samples were mixed with phosphate buffer (pH 7.4) prepared in D2O at a 2:1 ratio. Each spectrum was phased, baseline corrected and integrated using the Chenomx NMR Suite 7.1 (Chenomx Inc., Canada) software.

Cell stimulation, NFkB translocation and IL6 ELISA

Cells were stimulated with the complete cytokine mix (CCM) containing 10 ng/ml TNF-α, 10 ng/ml IL-1β, and 20 ng/ml IFN-γ (R&D Systems, Wiesbaden, Germany) or with its single components for 30 min in case of NFkB staining, 4 h for qPCR measurements, or 8 h for IL6 measurement in the respective medium. For NFkB measurement, cells were fixed, permeabilized and stained for NFkB. NFkB translocation was measured with the high throughput device Cellomics ArrayScan or CellInsight™ CX5 High Content Screening (Thermo Scientific) using the nuclear translocation algorithm as described previously (Henn

et al., 2011). Supernatants for IL6 ELISA were collected and stored at -80°C until further processing. IL6 was measured in supernatants diluted 1:5 in assay diluent and mouse IL-6 ELISA Ready-SET-Go was performed according to the manufacturer's protocol (eBioscience).

Results

Pivotal conditions for the generation of astrocytes from ESC-derived neural stem cells

Embryonic stem cells were differentiated within 7 days into neural stem cells of distinct morphologies, when plated on gelatin-coated dishes in N2B27-medium without growth factors. The cells had a high nestin expression and neurogenic potential as described previously (Conti et al., 2005; Zimmer et al., 2011a; Zimmer et al., 2011b). However, they hardly generated astrocytes when exposed to bone morphogenetic protein 4 (BMP4) (supplemental figure S1A), serum, CNTF or combinations thereof (not shown). The morphologically heterogeneous neural stem cell population contained bipolar cells in addition to other cell types (supplemental figure S1B/S3). Maintenance of the cells in EGF and FGF2-containing medium for several passages, and removal of aggregate-forming as well as flat, triangular cells (selective trypsinization/mechanical cleaning) at each passage step produced a homogeneous population of bipolar cells (supplemental figure S2). These 'secondary NSC' could be completely converted to GFAP-positive, nestin negative (about 80% of the cells only showed background staining after 3 days) astrocytes upon BMP4 exposure (supplemental figure S1A). The pivotal step in the production of 'murine astrocytes generated from embryonic stem cells' (mAGES) was the selection of an astrogenic cell population, which could then be easily maintained for at least 40 passages or frozen, banked, and re-thawed for subsequent differentiation (Fig. 1A).

The 'secondary NSC' (=high passage NSC) still retained their potential to generate mature neurons within 14 days, when growth factors were withdrawn from the medium (supplemental figure S4). Thus, NSC are multipotent neural stem cells, which give rise to astrocytes as well as neurons. This also held true for single cell clones: Ten out of 10 clones generated mAGES after 5 d of BMP4 exposure, with only slight morphological differences (supplemental figure S5). Moreover, when differentiated without growth factors, all of the clones generated about 60% neurons.

Astrogenic NSC have been produced five times from the mESC cell lines CGR8.0 and E14, and astrocytes have been generated from these with the same efficiency (not shown). Furthermore, mESC lines from a different mouse background (DO335 and BTBR) or murine induced pluripotent stem cells (iPSC) have been used successfully for mAGES generation (supplemental figure S6). Expression of GFAP, Aqp4, and nestin in mAGES produced therefrom was similar to the one found in the control line CGR8.0. This broad applicability confirmed the robustness of the astrocyte differentiation protocol.

Rapid generation of mature astrocytes from NSC

To characterize the cells, well-known markers were quantified for NSC as well as mAGES on mRNA level by quantitative PCR. Expression levels were compared to those of primary murine astrocytes. As previously reported, NSC expressed the neural stem cell markers *Nestin*, the brain lipid-binding protein *Blbp*, and the oligodendrocyte transcription factor *Olig2* (Conti et al., 2005). All three genes were downregulated in mAGES after differentiation for 5 days with BMP4 (Fig. 1B). The expression of *Blbp* and *Olig2* was similar in primary astrocytes and mAGES, while *Nestin* expression was more than 100 fold lower in mAGES compared to NSC or primary astrocytes. Other genes, which are normally expressed in both neural stem cells and astrocytes, like the glutamine synthetase (*Glul*) and the glutamate-aspartate transporter (*Glast*), were similarly expressed in all three cell types (Fig. 1B).

The astrocytic glial fibrillary acidic protein (*Gfap*) was highly expressed in mAGES as well as in primary astrocytes, whereas it was absent in NSC (Fig. 1C). The calcium-binding protein *S100b*, another well-known astrocyte marker, was highly expressed in all three cell types. Aquaporin 4 (*Aqp4*) and the glutamate transporter *Glt-1*, both specific markers for mature astrocytes, were upregulated in mAGES and primary astrocytes compared to NSC. Also, the aldehyde dehydrogenase *Aldh1L1*, which is reported to be astrocyte-specific in the brain (Cahoy et al., 2008), was expressed at 8-fold higher levels in mAGES compared to NSC (Fig. 1C).

When the time course of marker expression was followed during the conversion of NSC to mAGES, we found that dramatic changes (up to 1000-fold) occurred within 24 h after BMP4 addition. *Gfap* and *Glt-1* reached their maximum level already after 1 day, whereas *Aqp4* and *Nestin* further increased/decreased from day 1 to day 3 of BMP4 exposure. No changes were observed from day 3 to day 5. This suggests that astrocyte differentiation was completed after 3 days (Fig. 1D). The cells could be easily maintained in this stage for at least 4 weeks (not shown).

As further differentiation characteristic, we investigated the proliferation state of mAGES. This endpoint was chosen, because fully differentiated, mature astrocytes hardly undergo spontaneous cell division (i.e. without stimulation by growth factors or serum), while immature cells and astrocytic precursors (as sometimes present in primary cultures or stem cell-derived populations) have a relatively high proliferation rate. DNA replication was followed on single cell level by incorporation of the thymidine analogue 5-ethynyl-2'-deoxyuridine (EdU) into newly synthesized DNA. EdU was easily detected in the nuclei of NSC, whereas mAGES did not show any EdU incorporation at all during a 48 h incubation

(Fig. 1E). Exact quantification showed that more than 90% of NSC incorporated EdU (proliferating cells), while < 0.1% of mAGES proliferated (Fig. 1F).

Factors affecting differentiation efficacy

Since a single positive marker, such as *Gfap* mRNA or GFAP protein expression is not sufficient to characterize the extent of astrocyte differentiation, we chose here to measure GFAP, nestin (protein expression) and EdU incorporation (DNA synthesis) to compare different inducers of differentiation. BMP4, as used in our optimized protocol, led to a complete cell cycle exit, a high percentage of GFAP-positive cells and a > 80% reduction of nestin-positive cells. When fetal bovine serum (FBS) was used instead of BMP4, NSC differentiated to mAGES with a similar GFAP-expression, but nestin expression was higher (supplemental figure S7). Moreover, some mAGES were still proliferating, as indicated by EdU incorporation. Other cytokines, such as LIF or CNTF were not able to induce complete mAGES differentiation. Although GFAP was upregulated under these conditions to a high extent, the cells had a high nestin expression and proliferation rate. Moreover, the morphology was not typical of astrocytes (supplemental figure S7). These findings showed that GFAP alone is not sufficient to judge the differentiation to mature astrocytes, and that BMP4 was the most efficient agent, when several parameters were considered.

Finally, we were interested in whether the protocol allowed the identification of factors that negatively affect astrocyte differentiation (e.g. developmental toxicants). Several poisonous compounds known to affect neurodevelopment (e.g. methylmercury, manganese) were added during the differentiation procedure, and the expression (immunocytochemistry) of GFAP, Aqp4 and nestin was evaluated as endpoint. None of the toxicants affected mAGES generation, when used at non-cytotoxic concentrations. The same applied to small molecules, which are known to inhibit BMP4-induced SMAD-signaling (e.g. dorsomorphin or LDN-193189), indicating that canonical SMAD-signaling was not required for the differentiation of mAGES. From this we conclude that the protocol developed here is very robust towards many external disturbances. In the search for positive examples of developmental disturbances, we used two harsh approaches: (i) addition of noggin, which neutralizes BMP4, inhibited upregulation of GFAP as well as downregulation of nestin (data not shown); (ii) Very high concentrations of valproic acid (VPA, 10 mM), an HDAC inhibitor and neurodevelopmental toxicant, reduced mAGES generation, although they were not directly cytotoxic to astrocytes (supplemental figure S8). Thus, identification of chemicals or hormonal factors that inhibit astrocytogenesis seems to be feasible in this system.

Basic metabolic features of mAGES vs NSC

Relatively little is known yet about metabolic differences and similarities of astrocytes and their immediate precursors. In 2004, Brunet and others used murine neural stem cells differentiating to astrocytes in order to ask the question, at which developmental stage typical metabolic features of astrocytes are developed (Brunet et al., 2004). This elegant study provided initial evidence on metabolic differences between NSC and astrocytes. For example the maximum glutamate transport capacity changed during astrocytogenesis, but the line of work was unfortunately not continued and metabolic consequences for the cells are not known. As both mAGES and NSC expressed glutamine synthethase, we were interested in its cellular metabolic integration. As an integrative endpoint for this, we studied cell survival in medium supplemented with glutamine or not. In mAGES, the protein content per well (as viability parameter) and LDH release (as direct cell death measure) did not change within a 24 h period in either condition. Thus, the absence of glutamine did not trigger cell death (Fig. 2A and B). In fact, mAGES could be cultured for at least four days in glutamine-free medium without changes in viability (data not shown), confirming their independence from exogenous glutamine. By contrast, NSC were strongly dependent on glutamine, *i.e.* protein content per well decreased and LDH release increased already at 12 h after withdrawal from glutamine.

To get an overview on central energy metabolism, glucose uptake and lactate release rates were determined. NSC had nearly a two-fold metabolic rate (increased glucose consumption as well as lactate release) compared to mAGES (Fig. 2C and D). Altogether, both cell types had a high glucose to lactate conversion rate, and thus a minor contribution of mitochondrial metabolism (Fig. 2E,F), which is typical for stem cells (Candelario et al., 2013; Teslaa and Teitell, 2015), and astrocytes (Amaral et al., 2011; Magistretti et al., 1999; Waagepetersen et al., 1998). Thus, mAGES and NSC share some basic metabolic features, while differences became evident in glutamine-free environment, where only mAGES survived.

Immunocytochemical phenotyping of NSC and mAGES as homogeneous populations of neural stem cells and astrocytes

After having established basic metabolic features and mRNA marker expression patterns in NSC and mAGES cell populations, we investigated the homogeneity of the two cultures on single cell resolution by immunocytochemistry. While all NSC expressed NESTIN, most mAGES (>80%) down-regulated its expression to background levels, and some cells retained a weak expression. All NSC stained positive for the radial glia marker RC2, while this protein was absent in mAGES. GLAST was expressed to varying levels in NSC (heterogeneous

staining pattern), and to a much lower extent in mAGES. The calcium-binding protein S100B was detected in both cell types, consistent with similar mRNA levels (Fig. 3A).

The 'astrocytic' intermediate filament protein GFAP was strongly and ubiquitously (> 99%) expressed in mAGES, but not in NSC (< 1%). The same was observed for the glutamate transporter GLT-1. About 70 ± 7% of mAGES expressed AQP4 (to various extents), while this protein was absent in NSC. The morphology of NSC changed dramatically when exposed to BMP4 for 3 days. All of the small, bipolar NSC cells adopted the typical star-shaped / feathery morphology of astrocytes with radial processes and a flattened appearance, when differentiated to mAGES (Fig. 3B). To more closely examine the presence of astrocytic precursors, cells were stained for CD44 and A2B5, and both markers were undetectable in mAGES, while low levels of both proteins could be detected in NSC (Fig. 3C). The absence of the proliferation marker Ki67 in mAGES as well as the upregulation of p27, a cell cycle inhibitor in postmitotic cell, further confirmed their cell cycle exit and the absence of proliferating cells in this population. This characterization of the two cell populations, based on 12 different parameters, suggested that NSC were converted to a highly homogeneous population of astrocytes, containing no detectable proliferating precursor cells, or GFAP-negative cells, and displaying heterogeneity for Aqp4, as observed in brain tissue.

Whole transcriptome-based characterization of mAGES and their relationship to NSC

Only relatively recently, transcriptome data for astrocytes have become available to characterize their gene expression levels in different brain regions, culture conditions, and as opposed to neurons or oligodendrocytes (Cahoy et al., 2008; Lovatt et al., 2007; Shaltouki et al., 2013). However, little is known about the relationship of astrocytic and NSC gene expression, in particular for murine cells as major model system. Therefore, expression of over 34,000 genes (covered by 45,000 probesets) was measured here by microarray profiling. For each cell type (mAGES, NSC, mESC), mRNA was prepared from four independent differentiations, and principal component analysis of global gene expression revealed significant differences between all three cell types (Fig. 4A).

Quantitative comparison of gene expression allowed the identification of differentially expressed genes (DEG) for the different developmental stages, and more than 3,000 genes differed at least 2 fold between the cell types with an adjusted p-value cut-off < 0.05. The most substantial change occurred during mESC to NSC differentiation with more than 10,000 DEG between the two cell populations. Most importantly for the present study, we found that NSC and mAGES differed in more than 7,000 genes. Thus, although mAGES and NSC are

developmentally and functionally related, these data show their considerable disparity (Fig. 4B).

To identify marker genes, we performed pairwise comparisons of mESC, NSC and mAGES, and the top 20 up- or downregulated genes of each comparative analysis, sorted by p-value significance or fold change, were compiled (supplemental figure S10). During development of mESC to NSC, many genes involved in nervous system development were upregulated, some of them (e.g. *Olig1/2*, *Ptn* (pleiotrophin) or *Gpm6a* (calcium channel related to neurogenesis)) more than 1000-fold. The top 20 downregulated genes coded for factors essential for the maintenance of embryonic stem cells, such as *Zfp42*, *Nanog*, *Oct4* (*Pou5f1*), *Fgf4*, and *Lefty2* (supplemental figure S9).

The top 20 genes (according to the significance of regulation) in mAGES compared to NSC included *Id1* and *Id4*. These may not necessarily be cell type specific markers, as they are triggered by the BMP4 present in our cultures, but they are also known to play a role in astrocytogenesis (Fig. 4C). The highest upregulated gene in mAGES compared to NSC was fibromodulin (*Fmod*), which was more than 6,000-fold changed. The corresponding protein has metabolic functions and is involved in extracellular matrix organization. We also found genes involved in development (*Aplnr*, *Ndrg4*), chemotaxis (*Cxcr7*, *Cmtm6*), and immune response (*Lyz1*, *Lyz2*, *Peli2*). The top 10 upregulated genes were further validated by qPCR and the data confirmed that all of them were much higher expressed in mAGES compared to NSC (supplemental figure S12A/B). When DEG of mAGES against NSC were sorted by fold change, then the top 20 list comprised the well-known astrocyte marker genes *Gfap* and *Aqp4*. Furthermore, we found again genes involved in the heterogeneous functions of mature astrocytes, such as immune response, extracellular matrix organization, metabolic homeostasis, or angiogenesis. More than 70% of the genes, which were downregulated in mAGES vs NSC, were related to the cell cycle. This is well in concordance with the cell cycle exit of mAGES (Fig. 4C,D). Since the top 20 DEG expressed genes in mAGES comprised several transcripts, which were not previously recognized to be cell type specific, we investigated their *in vivo* expression by using published microarray data on parenchymal astrocytes and adult neural stem cells (aNSC) from the subventricular zone (Beckervordersandforth et al., 2010). Many of the genes upregulated in mAGES were also more prominent in mature astrocytes (supplemental figure S13A). Moreover, all genes found to be downregulated in our study were much higher expressed in aNSC than in parenchymal astrocytes . Thus, the set of DEG found in our study seems to be suitable to distinguish astrocytes and NSC also *in vivo*. In summary, the gene expression profiles provide cell type

specific signatures that enable a clear distinction between NSC and mAGES, and thus also a refined definition of respective cell-specific functions.

Comparison of mAGES gene expression with different other cell populations

For further characterization of mAGES and NSC, we compared their gene expression levels to legacy data and marker genes available from the literature. First, we compiled a list of genes specific for murine embryonic stem cells, neural stem cells, and astrocytes (Cahoy et al., 2008; Kuegler et al., 2010). Amongst the 94 markers, 29 were for embryonic stem cells, 29 were considered specific for neural stem cells, and 36 for astrocytes.

Comparison of mAGES, NSC and mESC expression levels for these markers showed that all embryonic stem cell marker genes were indeed expressed most strongly in our mESC cultures (Fig. 4E). About half of the genes considered to be specific for murine neural stem cells had their highest expression in NSC. However, the other half was expressed to similar levels in mAGES. Almost all astrocyte markers had indeed their highest expression in mAGES (compared to mESC or NSC), only *Glul* expression was more prominent in NSC (Fig. 4E).

These findings corroborate the formation of genuine astrocytes from NSC by the mAGES differentiation protocol presented here, and they also confirm a close biological relationship between astrocytes and NSC. The need for re-definition of an optimized marker set is also obvious from the data presented. For instance *Fgfr2* should rather be considered an astrocyte marker than an NSC marker.

To compare the microarray data of *in vitro* generated NSC and mAGES to primary brain cells, a heatmap of Spearman correlations was generated to illustrate relative similarities and differences of the expression profiles of the 94 marker genes described above. First, data on different primary cultures of astrocytes, neurons, or oligodendrocytes, prepared at different days of development (Cahoy et al., 2008), were correlated with NSC and mAGES. The mAGES correlated best with primary astrocytes, and less with primary neurons or oligodendrocytes. The highest correlation was found with astrocytes from postnatal brains at day 7-8 *post partum*. The NSC expression patterns only showed a modest correlation with any of the primary brain cells. They were most similar to developmentally early brain cells like postnatal astrocytes from *post partum* day 1 mice or oligodendrocyte precursor cells, while the greatest difference was found between NSC and mature astrocytes or neurons (Fig. 5A).

As an alternative approach, expression profiles of mAGES were also compared to data obtained previously on primary cells from different brain regions (Doyle et al., 2008). Here, the highest correlation was observed for cortical astrocytes, while intermediate correlations

were seen for cerebellar astrocytes and Bergmann glia, and the lowest correlation was obtained for neuronal cultures (Fig. 5B).

Divergent biosynthetic metabolism of NSC and mAGES

A direct metabolic comparison of neural stem cells and astrocytes has been difficult so far, especially as different populations of surrounding cells (in their tissue context or in conventional cultures) make biochemical approaches very challenging. We used here the availability of the homogeneous and well-characterized mAGES and NSC populations to obtain first evidence on divergent metabolic features of such cells. As an established approach to study central carbon metabolism, we followed the incorporation of the non-radioactive ^{13}C isotope from D-[1-^{13}C]-glucose into different cellular metabolites (Fig. 6A). As default condition, NSC and mAGES were cultured in medium, which was adapted to the respective basic cell functions in vivo: mAGES were cultured without glutamine, similar to conditions chosen for metabolic flux analysis with glutamine-producing primary astrocytes earlier (Amaral et al., 2011); NSC were cultured in the presence of 2 mM glutamine, according to their metabolic requirement for an external glutamine source (Fig. 2). The measurement of label incorporation into the cellular glucose pool and glycolytic metabolites (3-phosphoglycerate, phosphoenolpyruvate) confirmed for both cell types the high glycolytic rate: the equilibrium state for label incorporation rates (90% for glucose, 45% for the tricarbon metabolites) was reached within the first hour.

Analysis of the TCA cycle intermediate citrate showed a delayed equilibration of label incorporation at 12-24h (not shown), which is mainly due to a lower flux of glucose-derived pyruvate entering the TCA cycle compared to the high glycolytic flux, but also due to the large pools of (unlabeled) glutamate and aspartate in rapid exchange with TCA cycle intermediates. Still, the labeling of the citrate pool was faster and higher for NSC, suggesting differences in the metabolism of both cell populations (Fig. 6B). As citrate release is a well-known peculiar property of astrocytes (Westergaard et al., 1994), we quantified the citrate release rate from mAGES and NSC by quantitative ^{1}H-NMR spectroscopy (Figure 6C). NSC did not release significant amounts of citrate, while mAGES released citrate into the medium. A direct comparison with primary cortical astrocytes indicated that the overall range of their release-rate is similar to the one of mAGES (albeit still somewhat higher) (Figure 6C).

To investigate whether the observed differences in citrate release may have been due to medium conditions, we repeated experiments with mAGES in medium supplemented with 2 mM glutamine. Under these conditions, citrate release was even enhanced, compared to glutamine-free medium (used for the initial comparison). Conversely, NSC kept in glutamine-

free medium (instead of medium with 2 mM glutamine) did not show any citrate release (supplemental figure S14). Thus, citrate-release appears to be a unique cell-intrinsic difference in metabolism between mAGES and NSC.

For further characterization of the net uptake or release of medium components, the amino acid content of the supernatant was quantified 24 h after addition of fresh medium to the cells. NSC took up significant amounts of serine (Fig. 6D), while mAGES did not affect the concentrations of this amino acid to a measurable extent. The same pattern was observed for all branched chain amino acids: leucine, isoleucine (Fig. 6D) and valine were taken up by NSC, while mAGES did not contribute to a significant change of extracellular concentration. Net glutamate uptake was, however, more pronounced for mAGES than NSC.

The latter finding, based on long-term net uptake, was investigated in more biochemical detail, since the glutamate-glutamine shuttle between astrocytes and neurons plays an important role in brain physiology. Expression of glutamine synthetase and of the glutamate transporter GLAST by neural stem cells would in theory enable them to recycle glutamate, as in astrocytes, but this has not been tested directly. We evaluated therefore, as a first step, the glutamate uptake capacity by following the uptake of radiolabeled glutamate over a short period of time (8 min), and determining the initial speed for mAGES, NSC and primary astrocytes. All cells transported the amino acid to a relatively similar extent (Fig. 7A).

To obtain a measure of cellular glutamine synthesis under steady state conditions, we studied incorporation of ^{13}C from D-[1-^{13}C]-glucose into glutamine. The incorporation of parts of the glucose carbon skeleton into glutamine occurs via the citric acid cycle, α-ketoglutarate formation, transamination of this metabolite to glutamate and finally the glutamine synthetase reaction (Fig. 7B). This biosynthetic pathway is competitive with i) the direct uptake of glutamine and ii) with the uptake of glutamate and use of this non-labeled metabolite in the glutamine synthethase reaction. Thus, the relative extent of label incorporation from glucose allows conclusions on the existence and competition of these three reactions in the test cell population. For glutamine-free medium conditions (no glutamine uptake possible), we found that both NSC and mAGES synthesized glutamine (as indicated by ^{13}C-incorporation from glucose in about 20% of all glutamine). Thus, both cell types were capable of glutamine synthesis. When glutamine (2 mM) was added to the medium, neither mAGES nor NSC produced significant amounts of glutamine from labeled glucose, i.e. direct glutamine uptake was the dominating mechanism for filling the cellular glutamine pool (Fig. 7C). Thus, the cellular capacity of NSC (and mAGES) to synthesize glutamine (and the pathway employed for it) depends on the overall metabolic situation. When we re-examined the microarray data

for hints of metabolic differences relevant to glutamate metabolism, we found that pyruvate carboxylase expression was 19-fold up-regulated in mAGES compared to NSC. This enzyme catalyzes the anaplerotic process of oxaloacetate formation from pyruvate to replenish α-ketoglutarate in the TCA cycle, when this is used for glutamate and glutamine synthesis. In this context, pyruvate carboxylase has been reported to be astrocyte-specific (Schousboe et al., 2013; Shank et al., 1985), as it allows a higher efficacy of glutamine synthesis from glucose and TCA cycle metabolites in astrocytes.

As both NSC and mAGES were able to take up glutamate and to synthesize glutamine, we were interested in their ability to release glutamine to the medium. The net release/uptake was measured first in medium containing glutamine during a 24 h incubation period for the two cell types. Under these conditions, both mAGES and NSC showed a net consumption of the amino acid of similar magnitude (Fig. 7D). By contrast, cell type differences became obvious in glutamine-free medium: only mAGES released glutamine, whereas NSC did not release detectable amounts. Therefore, it appears that NSC cannot support the full glutamate-glutamine recycling between astrocytes and neurons, and they therefore differ in this respect from astrocytes/mAGES.

Functional maturity of mAGES concerning innate immune response and neuronal support

We tested also directly, in how far mAGES were able to provide neuronal support. Human neurons, differentiated from the conditionally-immortalized LUHMES cell line (Schildknecht et al., 2013; Scholz et al., 2011), were plated on top of mAGES. Within few days, stable co-cultures formed and mAGES assumed an extreme star-shaped morphology that is usually also observed for astrocytes present in primary rodent neuronal cultures (supplemental figure S15A). When medium changes were stopped 2 days after plating the neurons, all LUHMES in monocultures died within 10 days, whereas virtually all cells survived (and continued to do so for at least 4 weeks), when co-cultured with mAGES (supplemental figure S15B). Direct cell contact (of the somata) did not seem to be necessary for this effect, and a mAGES:LUHMES ratio as low as 1:5 seemed to be sufficient to support at least 80% neuronal survival (supplemental figure S15C). NSC did not appear to support LUHMES neuron survival, although the data interpretation from such experiments is difficult due to differentiation processes in the NSC population during the culture period. Moreover, LUHMES cultured on mAGES had an increased synaptic density compared to LUHMES mono-cultures (supplemental figure S16).

Besides metabolic functions pivotal for brain homeostasis, important roles of astrocytes also involve their activation in inflammatory situations (Falsig et al., 2006; Falsig et al., 2008), and

neuronal support (Kuegler et al., 2012). Therefore, we examined here whether mAGES acquire similar properties, and in how far they differ from NSC. First, mAGES and NSC were exposed to a mix of cytokines (complete cytokine mix (CCM): consisting of 10 ng/ml TNFα, 10 ng/ml IL1β, and 20 ng/ml IFNγ), which is normally found during brain inflammation, and is well-established to activate the inflammatory master transcription factor NFkB in glial cells (Henn et al., 2011; Kuegler et al., 2012). CCM triggered pronounced translocation of NFκB from the cytosol to the nucleus in mAGES, but showed no effect at all in NSC (Fig. 8A, supplemental figure S17). A more detailed investigation of the individual cytokines showed that translocation of NFκB was induced by TNFα as well as IL1β, but not by IFNγ (Fig. 8B). This activation pattern was similar to the one found before in primary astrocytes (Falsig et al., 2004; Henn et al., 2011), and in mAGES from different mESC and iPSC lines (supplemental Fig. S6).

Translocation of NFκB is an inflammation event easily quantifiable on single cell level, and indicating cytokine receptor activation. To obtain information on the actual inflammatory activation, it is necessary to measure relevant mRNA levels directly. Indeed, we found that CCM induced the expression of the cytokine *IL-6*, the inducible nitric oxide synthase *Nos-2*, and the toll-like receptor *Tlr-2* (Fig. 8C). All three exemplary marker genes used here, were upregulated in mAGES at 4 h after incubation with CCM at least 100-fold. NSC did not upregulate any of the genes when exposed to CCM (data not shown). For data on an actual functional response to inflammatory stimulation, we chose to measure IL-6 secretion by ELISA. Again, TNFα as well as IL1β, but not IFNγ, induced the production and the release of IL-6. On the level of protein secretion, there was an additive effect of the cytokines (Fig. 8D), exactly as described for primary astrocytes earlier (Falsig et al., 2004; Henn et al., 2011). NSC did not release any IL-6 when exposed to CCM (not shown). In summary, mAGES, but not NSC, responded to inflammatory cytokines, and the response pattern was consistent with that of primary astrocytes.

Discussion

The study of metabolic and functional features of astrocytes, in their resting state or in different defined activation scenarios, faces a number of challenges: i) measurements *in vivo* require a distinction of astrocytes from surrounding cells for the analytical endpoints chosen; ii) ex vivo studies, using e.g. FACS-purified adult astrocytes, suffer from a compromised viability of the obtained cells, and from undefined activation states, when put in culture; iii) *in vitro* studies mainly rely on studies of mixed populations, prepared from relatively immature cells. They may contain precursor cells, reactive astrocytes and other cell types, such as microglia. Additional approaches would thus be desirable to further explore astrocyte biology. In this study, we present such an alternative strategy that allows generation of a pure population of non-proliferative, non-activated astrocytes suitable for functional studies (neuronal support, inflammatory activation), investigation of metabolism (metabolite exchange, metabolic flux), and direct comparison to their immediate precursors, i.e. neural stem cells (NSC). The simultaneous availability of NSC, and of a population of non-proliferating astrocytes (mAGES) derived directly therefrom allowed us a direct comparison of the two cell types, and the identification of differences and similarities on the level of gene expression and intermediary metabolism (Fig. 9).

The heterogeneity of astrocytes derived from rodent brains or from stem cells has been underestimated in the past, as it has been common in the field to strongly rely on few single markers, such as GFAP. Nowadays, it is well described that there exist a subpopulation of mature GFAP-negative astrocytes, which express astrocyte marker genes apart from GFAP and reveal functional inflammatory capacity (Cahoy et al., 2008; Kuegler et al., 2012; Pekny et al., 1995; Walz and Lang, 1998). For many studies, a quantification of negative markers indicative of contaminating or immature cells is often missing. It is clear now that a single marker cannot define the cells (Gotz et al., 2015), and that functional properties (e.g. cell cycle progression, glutamate conversion or response to cytokines) need to be combined with an extensive set of markers. For instance, we found that GFAP-positive cells may co-express nestin or not, and also be proliferative or not, depending on the culture conditions. Such observation by us and others are in good agreement with findings that astrocytes generated from NSC by LIF, CNTF or FBS all expressed GFAP, but otherwise strongly differed from one another (Brunet et al., 2010). Here we found that the most complete conversion to non-dividing astrocytes occurred in the presence of BMP4, while addition of serum (FBS), which is frequently used in other protocols, exposes the cells to an undefined mixture of growth factors, some of which (e.g. EGF) also stimulate proliferation. The inevitable use of FBS in

conventional primary astrocyte cultures might therefore explain the heterogeneity of developmental stages in such cultures. Moreover many studies are not truly based on primary cells, but rather secondary or tertiary cultures. The associated selection and expansion of subpopulations, and cell activation may be the reason for contradictory studies on astrocytic inflammatory functions and makes it impossible to attribute specific metabolic functions unambiguously to primary mature astrocytes.

The absence of immature or reactivated cells in our cultures was indicated by the very strong downregulation of nestin as well as markers of immature astrocytes (A2B5, CD44). The maturity of mAGES was further confirmed by a cell cycle arrest (which persisted over weeks) in all cells in mAGES cultures. Moreover, we exclude the generation of quiescent stem cells, which may occur in some biological context as a consequence of the addition of BMP4 (Andreu et al., 2015; Martynoga et al., 2013; Mira et al., 2010): The quiescent stem cell marker CD133/prominin1 was not expressed in mAGES (supplemental figure S18) and the cells did not re-enter the cell cycle when exposed to EGF or sonic hedgehog (SHH) within 10 days of exposure, as it would be expected from quiescent stem cells (Codega et al., 2014). As the procedure we describe here was reproducible for several lines of ESC or for iPSC, and as large numbers of cells can be produced by this protocol in a fast and cost-efficient way, mAGES are suggested here as valuable additional model system to study the cell biology (e.g. epigenetics, metabolic adaptation, inflammation, gene regulation, or cell cycle re-activation) of astrocytes. Generation of mAGES from BTBR ESC, i.e. from a mouse strain used for autism studies (McFarlane et al., 2008), shows that the protocol is suitable also for the study of genetic modifications underlying disease.

For the study of human genes contributing to disease, it would be desirable to transfer the protocol to human cells. At the present stage, we cannot predict whether this will be possible with the same speed and efficiency as found in the murine system. The key factor for the efficient and rapid differentiation of mAGES was the generation of the right type of precursors. To our knowledge the human equivalent has not yet been found, despite large efforts. Several protocols to generate astrocytes from human ESC or iPSC have been published (Gupta et al., 2012; Juopperi et al., 2012; Krencik et al., 2011; Sun et al., 2008). They often require excessively long differentiation times (> 3 months), and the obtained cell populations usually contain substantial amounts of precursors or other cell types. For instance, a recent, very efficient protocol developed by experienced specialists in the field generated purities of 70-80% at best (Shaltouki et al., 2013). Such cells have been used successfully for transcriptome profiling, but long-term studies and investigations in metabolic pathways might

be complicated by other cells present. Even cells offered commercially from the best-known source for stem cell derived products (Cellular Dynamics iCell astrocytes; www.cellulardynamics.com/products/astrocytes.html) are very strongly proliferative. A recent advance may be the generation of 'late radial glia cells' as precursor population. This protocol allowed then the generation of up to 88% GFAP-positive cells within 7 days of the addition of BMP4 (Duan et al., 2015). Although this latter procedure, close to the one presented here for mAGES, sounds promising, there are some issues that need to be resolved: the generation of the right precursors takes over 100 days; it is not yet clear, whether these precursor cells have sufficient proliferative and self-renewal capacity to allow astrocyte generation at a reasonable cost; and it is not clear whether the astrocytes generated show the required functional features and are non-dividing. An exact definition of the required precursor cell population in the mouse system may help to guide protocol optimization for human cells. To obtain the required data, it may be helpful to compare the transcript profile of NSC of the present study to NSC we have used earlier for the generation of murine embryonic stem cell-derived astrocytes (MEDA). The latter protocol (Kuegler et al., 2012) generated astrocyte cultures with a large proportion of mature astrocytes, but also with subpopulations of immature cells and rapidly dividing cells (i.e. similar to the situation usually observed in the currently available human stem cell-derived astrocytes). A better selection of the precursors by repeated selective passaging of the desired subpopulation, made all the difference in the speed, efficacy and homogeneity of the mAGES generation. Thus, knowledge of differentially expressed genes or surface markers for the desired start population is expected to accelerate such a process for human cells. We hope that the detailed description of the pivotal protocol steps of mAGES generation not only helps the implementation of mAGES in the research community, but would also support the optimization of protocols for human astrocytes.

The availability of mAGES and NSC in highly homogeneous cultures allowed comparisons of their metabolic characteristics. Earlier studies found expression of glutamate transporters as well as the glutamine synthetase in both cell types. The functionality of NSC glutamate transporters was then shown in short-term biochemical D-aspartate uptake experiments (Brunet et al., 2004). Our cultures provided now an experimental basis for steady state studies (as part of cellular homeostasis) on the role of glutamate uptake/glutamine release during prolonged culture times. This allowed conclusions on the role that NSC may take part in glutamate-glutamine recycling. The finding that both NSC and mAGES were able to take up glutamate and convert it to glutamine suggests that neural stem cells resemble astrocytes in this metabolic function. However, NSC did not release glutamine to the extracellular space as

mAGES did. Thus, NSC are probably not involved in the glutamate-glutamine shuttle between astrocytes and neurons. However, glutamine synthetase activity is also essential for detoxification of excessive ammonia in the brain. NSC may take part in this important process.

A further metabolic difference of mAGES and NSC concerned the release of citrate to the extracellular space. This peculiar metabolic feature has been known for astrocytes (Westergaard et al., 1994), and was now confirmed for the highly homogeneous mAGES cultures, while this process was not detected in NSC. Furthermore, NSC clearly differed from mAGES by their net exchange pattern for various amino acids. The interpretation of such metabolic studies requires homogeneous populations to exclude subpopulations responsible for altered overall metabolite patterns. The data generated here suggest that the cultures are suitable for more extensive mapping of overall cellular metabolic fluxes, and for the comparison of such data to primary astrocyte cultures (Amaral et al., 2011) and other cell types.

In the fields of immunology and stem cell biology, it has long become a rule that cells cannot be characterized by single markers, but rather by signatures across multiple positive and negative markers. The recognition of astrocyte heterogeneity has now led to a critical reexamination of the specificity of established marker genes in the field of neurosciences. Microarray studies provide new insight in corresponding multifactorial marker patterns of glial cells (Beckervordersandforth et al., 2010; Gotz et al., 2015). Classical single markers, such as GFAP, may still play a role in the distinction of neurons or microglia from astrocytes, but multiple markers and full expression profiles are required to characterize closely related cell populations. This is the case for a comparison between astrocytes and their self-renewing precursors, as presented here. The gene expression data generated in this study can be used to define a predictive set of differentially expressed genes for in vitro differentiation experiments in different settings. Such marker selection benefits largely from earlier gene expression studies of different murine cell populations that helped to define commonalities and differences of astrocytes from different brain regions, developmental stages and activation states (Beckervordersandforth et al., 2010; Buffo et al., 2008; Cahoy et al., 2008; Dimou and Gotz, 2014; Lovatt et al., 2007). *In vitro*, such studies have in the past been mainly used to define cell activation states (Falsig et al., 2006; John et al., 2005), while less information is available on the ground state of murine astrocytes cultures as opposed to other cell types. Here, we used microarray analysis to explore differentially-expressed genes between NSC, mAGES and pluripotent ESC similarly to what has been done for human cells (Shaltouki et

al., 2013). Moreover, the data were used for comparisons to some available data sets on astrocytes. As our system provides the opportunity to directly compare mAGES to their immature precursors, new RNA markers of mature cells such as fibromodulin (*Fmod)* could be readily identified (Fig. 9). The cognate protein (fibromodulin) is involved in extracellular matrix organization, which is one of the first recognized and accepted functions of astrocytes that has been described in connection with astrocytes functioning as 'brain glue' (Volterra and Meldolesi, 2005).

Since differentiation of mAGES is very fast, and all steps are easily accessible at every stage, it offers the possibility to investigate factors and e.g. toxicants or drugs that disturb astrocyte generation. For instance, valproic acid (VPA) has been shown to disturb astrocyte generation, while it favors neurogenesis (Su et al., 2014). We confirmed this property in a study that examined the generation of mAGES with readouts of maturity markers on the single cell level. Our system can thus be used for high throughput screenings of developmental toxicants, or for general studies of astrocyte development, for instance with regard to gene regulation, acquisition of immune functions and of biological features controlling the expression of cytokine receptors.

The differentiation of mAGES from different iPSC lines offers new possibilities to investigate the involvement of astrocytes in processes leading to disease establishment or progression. Such approaches have already been taken with astrocyte-enriched cultures derived from human iPSC with a Huntington's disease genetic background (Juopperi et al., 2012), or a Rett syndrome genotype (Lioy et al., 2011). The availability of a wealth of transgenic and gene-targeted mice, or the possibility of direct manipulation of NSC or mAGES offers multiple opportunities for the study of disease-related genes. Besides such studies, the inflammation competence of mAGES might be utilized to study the causes and consequences of astrocyte activation in multiple neurological diseases. Moreover, the easy availability of the cells, and their compatibility with e.g. human neuronal cultures allows also investigations of neuroprotective or neuro-damaging roles of astrocytes (Efremova et al., 2015; Schildknecht et al., 2015).

In summary, our exact characterization of the differentiation requirements, together with data on the phenotype and function of the resultant cells, suggests that generation of astrocytes from pluripotent stem cells (mAGES) is a viable alternative to the preparation of primary astrocytes for biological, pharmacological and toxicological studies. The direct comparison of mAGES and NSC performed here provided new insights into astrocyte and neural stem cell

metabolism. In the future, the generation of mAGES with different genetic backgrounds opens up new possibilities in biomedical research.

Figure legends

Figure 1: Rapid generation of non-proliferating, mature astrocytes from neural stem cells.

(**A**) A heterogeneous population of 'neural stem cells' (d7NSC) was generated within 7 days by spontaneous differentiation of murine embryonic stem cells (mESC). Selective passaging (at least 8-12 times) in the presence of 20 ng/ml EGF and FGF2 on gelatine produced a homogeneous population of NSC that could be frozen for later use or maintained by further passaging. Transfer of the cells to poly-ornithin/laminin (P/L)-coated dishes and exposure to BMP4 (20 ng/ml) resulted in the generation of murine astrocytes generated from mESC (mAGES). (**B,C**) For measurements of gene expression by qPCR, mRNA was prepared from mAGES (after 5 days of differentiation), NSC or primary murine astrocytes. All data are given in fold difference (x-fold) relative to the housekeeping gene *Gapdh* (note logarithmic axis scaling). The horizontal brackets in the plots indicate the fold-difference of mAGES vs NSC (**B**) Nestin, Blbp (FABP7, brain lipid binding protein), Olig2 (oligodendrocyte lineage transcription factor; neuroectodermal marker), Glul (Glutamine synthetase) and Glast (Slc1A3; glutamate transporter) were used as NSC markers; (**C**) Gfap (glial fibrillary acidic protein), S100b (S100beta), Aqp4 (aquaporin), Glt-1 (Slc1A2, glutamate transporter), and Aldh1L1 (aldehyde dehydrogenase) were used as astrocyte markers (**D**) NSC were exposed to 20 ng/ml BMP4 and left to differentiate to mAGES. At the times indicated, mRNA was prepared to quantify the expression of marker genes by qPCR. All data are given relative to the expression in NSC (log_{10}-scaled), based on the $\Delta\Delta C_T$ method. Data are means ± SEM from three experiments (some error bars are smaller than the symbols). *** $p < 0.0001$; ** $p < 0.001$; * $p < 0.01$ (One-way-ANOVA with Dunnett's posthoc test). (**E**) NSC and mAGES (3 days old) were incubated with the nucleoside analogue EdU (10 μM) for 48 h, before cells were fixed. Then, EdU incorporation was visualized by immunocytochemistry, and nuclei were counterstained with H-33342 (note that EdU staining (dark green) appears yellow to green, depending on the strength of the always underlying H-33342 (red) stain) (**F**) The number of nuclei that were EdU-positive were counted in NSC and mAGES cultures by an automated screening microscope (1000 nuclei/condition). The data displayed are means ± SEM from three independent experiments. In mAGES cultures less than 1 cell per condition was found to be EdU-positive (<0.1%).

Figure 2. General metabolic features of mAGES vs NSC

(**A**) Cells (mAGES/NSC) were plated in 6 well plates at a density of 500,000 cells/well for mAGES and 80,000 cells/well for NSC. After 48 h (5 days for mAGES) the plating medium was changed, and cells were cultured further in medium containing either 2 mM glutamine

(Gln) or no Gln. At the times indicated, medium was removed, cells were lysed and the protein content was measured. (**B**) The experiment was performed as in (A), and at the times indicated the percentage of LDH released from the cells into the medium was measured as cell death parameter. (**C, D**) The glucose concentration or lactate concentration in the medium of NSC and mAGES cultures was measured over time, and the overall protein content of the cultures was determined. From these data, normalized uptake/release rates were calculated. Data presented are means ± SEM of three separate experiments. (**E**) The central carbon metabolism was schematically summarized to indicate that the uptake of 1 mol of glucose would result in the average release of two mol lactate, if only glycolytic catabolism was involved; and less than 2 mol lactate if some of the glucose metabolites were used in the tricarboxylic acid cycle (TCA) to produce CO_2. (**F**) The data from (C+D) were used to calculate the lactate to glucose ratio of NSC and mAGES metabolism.

Figure 3. Immunocytochemical characterization of marker expression and cell culture homogeneity of NSC and mAGES.

NSC and mAGES (3 days old) were fixed and permeabilized. Marker proteins (green) were visualized by immunocytochemistry and nuclei were counterstained with H-33342 (red). (**A**) NESTIN, RC2 (radial glia marker), GLAST (glutamate transporter), and S100B were used as NSC marker proteins. (**B**) GFAP (glial fibrillary acidic protein), AQP4 (aquaporin 4), and GLT-1 (glutamate transporter) were used as markers for mature astrocytes. Phase contrast pictures were taken from living cells before fixation. (**C**) CD44 and A2B5 were used as astrocyte-precursor markers. The cell cycle inhibitor (p27) and the proliferation marker Ki67 were used to examine the cell cycle status of NSC and mAGES.

Figure 4. Transcriptome data of mESC, NSC and mAGES and comparative analysis of gene expression to identify mature astrocyte marker genes

RNA was prepared from mESC, NSC, and mAGES (5 days old) in 4 independent experiments and used for Affymetrix Mouse Genome 430 2.0 arrays. (**A**) To visualize the grouping patterns across different samples, a principal component analysis of global gene expression was performed for samples of 4 independent differentiations, and data (colour coded) with their 95% confidence interval (grey shading) were plotted along the first two principal components (PC). (**B**) Gene expression datasets from (A) were used to compute differentially-expressed genes (DEG) by applying the Empirical Bayes moderated t-statistics and adjusting for multiple hypothesis testing using the Benjamini-Hochberg method. Genes with $\geq$ 2-fold changes and an adjusted p-value < 0.05 were considered as significant (with duplicates or non-annotated transcripts removed). The number of DEG is shown for different

pairwise comparisons (e.g. mAGES vs NSC) separately for up-regulations (up, red) and down-regulations (down, blue). (**C**) The gene list generated in (B) was sorted by adjusted p-value and the top 20 genes that were differentially expressed in mAGES relative to NSC are displayed. Bars indicate fold changes of genes, which were up-regulated (red) or down-regulated (blue). (**D**) The gene list generated in (B) was sorted by fold change and the top 20 DEG are presented. The adjusted p-value of all selected genes was $< 10^{-5}$. (**E**) The gene expression values were retrieved for 94 genes selected from the literature as being specific for embryonic stem cells, neural stem cells, or astrocytes (listed vertically). The normalized expression data on log-scale obtained here (4 times mESC, 4 x NSC, 4 x mAGES) are plotted as horizontal lines of the heatmap in the form of z-scores (blue color representing low and red color high expression). The corresponding gene expression values are listed in supplemental figure S11.

Figure 5. Correlation of mAGES microarray profiles with published data on astrocytes and other brain cell types.

(**A**) The heatmap shows the Spearman correlation coefficient between NSC and mAGES (vertical axis) and data published by Cahoy et al. (2008) on primary astrocytes, neurons, or oligodendrocytes, isolated at different postnatal days (horizontal axis). (**B**) The heatmap shows the Spearman correlation coefficient between mAGES (vertical axis) and data from Doyle et al. (2008) on primary astrocytes from different brain regions, neurons, or oligodendrocytes (horizontal axis). The Spearman correlation was performed over the 94 selected genes (Fig. 4E). Blue color represents low correlation and red color high correlation (highest red value = 0.8 in both cases). Samples are grouped by cell type across both studies; within the sample groups, the ordering was determined by a standard average linkage hierarchical clustering using the Euclidean distance metric.

Figure 6. Differences in metabolic flux between NSC and mAGES

(A) Schematic representation of ^{13}C incorporation into citrate from D-[1-^{13}C]-glucose. The carbon skeleton of selected metabolites is shown. Citrate can incorporate ^{13}C at one carbon position (M+1), which is C2, from condensation of [2-^{13}C]-acetyl-CoA with unlabeled oxaloacetate. The M+2 citrate isotopomer is generated, when [2-^{13}C]-citrate is used in the tricarboxylic acid (TCA) cycle to generate [2-^{13}C]-oxaloacetate, which condenses with [2-^{13}C]-acetyl-CoA, yielding double-labeled [2,3-^{13}C]-citrate. NB: Not shown here is that citrate might alternatively be labeled at C4 depending on label position in oxaloacetate at C3 (due to symmetric structure of fumarate). **(B**) Cells (mAGES/NSC) were plated in 6 well plates at a density of 500,000 cells/well for mAGES and 80,000 cells/well for NSC. After 48 h (5 days

for mAGES), medium was changed to glucose-free medium supplemented 10 mM D-[1-^{13}C]-glucose. Supernatant as well as cell extracts were harvested at indicated time points. ^{13}C-incorporation into citrate was measured in NSC and mAGES cell extracts after derivatization and analysis by gas chromatography-mass spectrometry (GC-MS). Isotopomer fractional enrichment above natural abundance of 1.2% (i.e. the percentage of the respective isotopomer of the total citrate pool) was measured for M+1 (= citrate with one ^{13}C), and M+2 (= citrate with two ^{13}C atoms). (**C**) Experiments were performed as in (B) and citrate concentrations were measured in the supernatants of NSC and mAGES using ^{1}H-NMR spectroscopy. For comparison, data from cortical astrocyte cultures were included. The overall protein content was measured in pellets of cell extracts, and the citrate release was normalized accordingly. (**D**) Experiments were performed as in (B) and serine, leucine, and isoleucine were measured in NSC and mAGES supernatants by HPLC. The overall protein content was measured in pellets of cell extracts, and amino acid uptake or release rates were calculated. All data are means ± SEM from duplicate determinations in three independent experiments. ***$p < 0.001$ (One-way-ANOVA with Dunnett's posthoc test).

Figure 7. Similarities and differences of NSC and mAGES concerning metabolic processes related to the glutamate-glutamine cycle

(**A**) NSC, mAGES (5 days old), and primary astrocytes were incubated with glutamate (10 µM, radiolabeled (^{3}H) with 0.12 µCi/well) in PBS for 8 minutes. After 3 rapid washing steps with PBS, cells were lysed and the cellular glutamate content was measured using a scintillation counter. The uptake data were normalized to mAGES as 100% reference point. (**B**) Schematic representation of ^{13}C incorporation into glutamate and glutamine from D-[1-^{13}C]-glucose: the carbon skeleton of selected metabolites is shown. Direct metabolism of glucose to pyruvate → acetyl-CoA → citrate → α-keto-glutarate can lead to the formation of glutamine with one ^{13}C-atom incorporated at positon C4 (M+1). Use of the already singly-labeled tricarboxylic acid (TCA) cycle metabolite [2-^{13}C]-oxaloacetate in the citrate synthase reaction can lead to the formation of double-labeled [2,3-^{13}C]-citrate. This can then be further metabolized to double labeled α-keto-glutarate, [3,4-^{13}C]-glutamate and [3,4-^{13}C]-glutamine (M+2). (**C**) Cells (mAGES/NSC) were plated in 6-well plates at a density of 500,000 cells/well for mAGES and 80,000 cells/well for NSC. After 48 h (5 days for mAGES), medium was changed to glucose-free medium supplemented with 10 mM D-[1-^{13}C]-glucose with either 2 mM glutamine (Gln) or no Gln. Supernatants and cell extracts were harvested at 0.3, 3, 12, and 24 h. 13C-incorporation into glutamine was measured by gas chromatography-mass spectrometry (GC-MS) in NSC and mAGES cell extracts. Isotopomer fractional

enrichment (i.e. the percentage of the respective isotopomer of the total glutamine pool) was measured over time for M+1 (= glutamine with one ^{13}C), and M+2 (= glutamine with two ^{13}C atoms). It is displayed here for the 12 h incubation (= steady-state level). (**D**) Experiments were performed as in (C) and supernatants were harvested at 12 h. Glutamine concentrations were measured by HPLC. The overall protein content was measured in pellets of cell extracts, and the uptake or release rate were calculated (similar results were obtained at 24 h). All data are means ± SEM from three independent experiments, * $p < 0.01$ (One-way-ANOVA with Dunnett's posthoc test).

Figure 8. Response of mAGES, but not NSC, to inflammatory stimulation.

(**A**) NSC and 5 days old mAGES were exposed to complete cytokine mix (CCM, 10 ng/ml TNFα, 10 ng/ml IL1β, and 20 ng/ml IFNγ) for 30 min. Then, cells were fixed, permeabilized, and immunostained for the p65 unit of the inflammatory transcription factor NF-κB (NFkB). Nuclei were counterstained with H-33342. The ratio of NFkB in the cytosol and the nucleus was measured in NSC and mAGES cultures by an automated screening microscope (1000 nuclei/condition) and an image data processing procedure based on a validated algorithm. The percentage of cells with NFkB translocation into the nuclei was calculated and presented. See supplemental figure S17 for representative images. (**B**) NFkB translocation was determined as in (A) for mAGES exposed to CCM or its single components for 30 min. (**C**) Primary astrocytes and mAGES were stimulated with CCM, and mRNA was isolated 4 h later from control and stimulated cells. The expression of three inflammatory markers (IL-6; inducible nitric oxide synthase (iNOS); toll-like receptor-2 (TLR2) was analyzed by qPCR. Data are given for CCM-exposed cells relative to the expression in unstimulated control cells. (**D**) mAGES were exposed to CCM for 8 h. Supernatants were harvested, and IL6 protein was measured by ELISA. All data are means ± SEM from three independent experiments.

Figure 9. Summary of differences and similarities between NSC and mAGES

NSC (blue) and mAGES (red) show functional differences as well as similarities (intersection, purple). Gene expression profiles based on microarray profiling are listed below. The specific marker genes suggested below are (i) known NSC or astrocyte markers (see Fig. 4E); (ii) had a logarithmic mean expression value higher than 4 in one of the cell types (to avoid genes with borderline expression); (iii) and showed a difference in their logarithmic mean expression values (mAGES vs NSC) higher than 1.8 (3.48-fold difference). 'New genes' comprise the top DEG between NSC and mAGES, which were validated by qPCR. *: genes labelled with asterisk were found here to show expression differences of 3.5-fold between

mAGES and NSC, but they have previously been discussed as potential markers for the other cell type than the one listed here (i.e. their specification was revised by our study).

References

Amaral AI, Teixeira AP, Hakonsen BI, Sonnewald U, Alves PM. 2011. A comprehensive metabolic profile of cultured astrocytes using isotopic transient metabolic flux analysis and C-labeled glucose. Front Neuroenergetics 3:5.

Andreu Z, Khan MA, Gonzalez-Gomez P, Negueruela S, Hortiguela R, San Emeterio J, Ferron SR, Martinez G, Vidal A, Farinas I and others. 2015. The cyclin-dependent kinase inhibitor p27 kip1 regulates radial stem cell quiescence and neurogenesis in the adult hippocampus. Stem Cells 33:219-29.

Bayraktar OA, Fuentealba LC, Alvarez-Buylla A, Rowitch DH. 2015. Astrocyte development and heterogeneity. Cold Spring Harb Perspect Biol 7:a020362.

Beckervordersandforth R, Tripathi P, Ninkovic J, Bayam E, Lepier A, Stempfhuber B, Kirchhoff F, Hirrlinger J, Haslinger A, Lie DC and others. 2010. In vivo fate mapping and expression analysis reveals molecular hallmarks of prospectively isolated adult neural stem cells. Cell Stem Cell 7:744-58.

Benjamini Y, Hochberg Y. 1995. Controlling the false discovery rate: a practical and powerful approach to multiple testing. Journal of the Royal Statistical Society Series B (Methodological):289-300.

Brunet JF, Allaman I, Magistretti PJ, Pellerin L. 2010. Glycogen metabolism as a marker of astrocyte differentiation. J Cereb Blood Flow Metab 30:51-5.

Brunet JF, Grollimund L, Chatton JY, Lengacher S, Magistretti PJ, Villemure JG, Pellerin L. 2004. Early acquisition of typical metabolic features upon differentiation of mouse neural stem cells into astrocytes. Glia 46:8-17.

Buffo A, Rite I, Tripathi P, Lepier A, Colak D, Horn AP, Mori T, Gotz M. 2008. Origin and progeny of reactive gliosis: A source of multipotent cells in the injured brain. Proc Natl Acad Sci U S A 105:3581-6.

Cahoy JD, Emery B, Kaushal A, Foo LC, Zamanian JL, Christopherson KS, Xing Y, Lubischer JL, Krieg PA, Krupenko SA and others. 2008. A transcriptome database for astrocytes, neurons, and oligodendrocytes: a new resource for understanding brain development and function. J Neurosci 28:264-78.

Candelario KM, Shuttleworth CW, Cunningham LA. 2013. Neural stem/progenitor cells display a low requirement for oxidative metabolism independent of hypoxia inducible factor-1alpha expression. J Neurochem 125:420-9.

Codega P, Silva-Vargas V, Paul A, Maldonado-Soto AR, Deleo AM, Pastrana E, Doetsch F. 2014. Prospective identification and purification of quiescent adult neural stem cells from their in vivo niche. Neuron 82:545-59.

Conti L, Pollard SM, Gorba T, Reitano E, Toselli M, Biella G, Sun Y, Sanzone S, Ying QL, Cattaneo E and others. 2005. Niche-independent symmetrical self-renewal of a mammalian tissue stem cell. PLoS Biol 3:e283.

Crocker SJ, Frausto RF, Whitton JL, Milner R. 2008. A novel method to establish microglia-free astrocyte cultures: comparison of matrix metalloproteinase expression profiles in pure cultures of astrocytes and microglia. Glia 56:1187-98.

Daikhin Y, Yudkoff M. 2000. Compartmentation of brain glutamate metabolism in neurons and glia. J Nutr 130:1026S-31S.

Delaney CL, Brenner M, Messing A. 1996. Conditional ablation of cerebellar astrocytes in postnatal transgenic mice. J Neurosci 16:6908-18.

Dimou L, Gotz M. 2014. Glial cells as progenitors and stem cells: new roles in the healthy and diseased brain. Physiol Rev 94:709-37.

Doetsch F, Caille I, Lim DA, Garcia-Verdugo JM, Alvarez-Buylla A. 1999. Subventricular zone astrocytes are neural stem cells in the adult mammalian brain. Cell 97:703-16.

Doyle JP, Dougherty JD, Heiman M, Schmidt EF, Stevens TR, Ma G, Bupp S, Shrestha P, Shah RD, Doughty ML and others. 2008. Application of a translational profiling approach for the comparative analysis of CNS cell types. Cell 135:749-62.

Duan L, Peng CY, Pan L, Kessler JA. 2015. Human pluripotent stem cell-derived radial glia recapitulate developmental events and provide real-time access to cortical neurons and astrocytes. Stem Cells Transl Med 4:437-47.

Efremova L, Schildknecht S, Adam M, Pape R, Gutbier S, Hanf B, Burkle A, Leist M. 2015. Prevention of the degeneration of human dopaminergic neurons in an astrocyte co-culture system allowing endogenous drug metabolism. Br J Pharmacol 172:4119-32.

Eng LF, Ghirnikar RS, Lee YL. 2000. Glial fibrillary acidic protein: GFAP-thirty-one years (1969-2000). Neurochem Res 25:1439-51.

Falsig J, Latta M, Leist M. 2004. Defined inflammatory states in astrocyte cultures: correlation with susceptibility towards CD95-driven apoptosis. J Neurochem 88:181-93.

Falsig J, Porzgen P, Lund S, Schrattenholz A, Leist M. 2006. The inflammatory transcriptome of reactive murine astrocytes and implications for their innate immune function. J Neurochem 96:893-907.

Falsig J, van Beek J, Hermann C, Leist M. 2008. Molecular basis for detection of invading pathogens in the brain. J Neurosci Res 86:1434-47.

Gotz M, Sirko S, Beckers J, Irmler M. 2015. Reactive astrocytes as neural stem or progenitor cells: In vivo lineage, In vitro potential, and Genome-wide expression analysis. Glia 63:1452-68.

Gupta K, Patani R, Baxter P, Serio A, Story D, Tsujita T, Hayes JD, Pedersen RA, Hardingham GE, Chandran S. 2012. Human embryonic stem cell derived astrocytes mediate non-cell-autonomous neuroprotection through endogenous and drug-induced mechanisms. Cell Death Differ 19:779-87.

Hansson E. 1986. Primary astroglial cultures. A biochemical and functional evaluation. Neurochem Res 11:759-67.

Henn A, Kirner S, Leist M. 2011. TLR2 hypersensitivity of astrocytes as functional consequence of previous inflammatory episodes. J Immunol 186:3237-47.

Hernández C, Martín M, Bodega G, Suárez I, Pérez J, Fernández B. 1999. Response of carp central nervous system to hyperammonemic conditions: an immunocytochemical study of glutamine synthetase (GS), glial fibrillary acidic protein (GFAP) and 70 kDa heat-shock protein (HSP70). Aquat Toxicol 45:195-207.

Ihaka R, Gentleman R. 1996. R: a language for data analysis and graphics. Journal of computational and graphical statistics 5(3):299-314.

Ihrie RA, Alvarez-Buylla A. 2008. Cells in the astroglial lineage are neural stem cells. Cell Tissue Res 331:179-91.

John GR, Lee SC, Song X, Rivieccio M, Brosnan CF. 2005. IL-1-regulated responses in astrocytes: relevance to injury and recovery. Glia 49:161-76.

Juopperi TA, Kim WR, Chiang CH, Yu H, Margolis RL, Ross CA, Ming GL, Song H. 2012. Astrocytes generated from patient induced pluripotent stem cells recapitulate features of Huntington's disease patient cells. Mol Brain 5:17.

Kacem K, Lacombe P, Seylaz J, Bonvento G. 1998. Structural organization of the perivascular astrocyte endfeet and their relationship with the endothelial glucose transporter: a confocal microscopy study. Glia 23:1-10.

Krencik R, Weick JP, Liu Y, Zhang ZJ, Zhang SC. 2011. Specification of transplantable astroglial subtypes from human pluripotent stem cells. Nat Biotechnol 29:528-34.

Kriegstein A, Alvarez-Buylla A. 2009. The glial nature of embryonic and adult neural stem cells. Annu Rev Neurosci 32:149-84.

Krug AK, Kolde R, Gaspar JA, Rempel E, Balmer NV, Meganathan K, Vojnits K, Baquie M, Waldmann T, Ensenat-Waser R and others. 2013. Human embryonic stem cell-derived test systems for developmental neurotoxicity: a transcriptomics approach. Arch Toxicol 87:123-43.

Kuegler PB, Baumann BA, Zimmer B, Keller S, Marx A, Kadereit S, Leist M. 2012. GFAP-independent inflammatory competence and trophic functions of astrocytes generated from murine embryonic stem cells. Glia 60:218-28.

Kuegler PB, Zimmer B, Waldmann T, Baudis B, Ilmjarv S, Hescheler J, Gaughwin P, Brundin P, Mundy W, Bal-Price AK and others. 2010. Markers of murine embryonic and neural stem cells, neurons and astrocytes: reference points for developmental neurotoxicity testing. ALTEX 27:17-42.

Levitt P, Rakic P. 1980. Immunoperoxidase localization of glial fibrillary acidic protein in radial glial cells and astrocytes of the developing rhesus monkey brain. J Comp Neurol 193:815-40.

Lioy DT, Garg SK, Monaghan CE, Raber J, Foust KD, Kaspar BK, Hirrlinger PG, Kirchhoff F, Bissonnette JM, Ballas N and others. 2011. A role for glia in the progression of Rett's syndrome. Nature 475:497-500.

Liu X, Bolteus AJ, Balkin DM, Henschel O, Bordey A. 2006. GFAP-expressing cells in the postnatal subventricular zone display a unique glial phenotype intermediate between radial glia and astrocytes. Glia 54:394-410.

Lovatt D, Sonnewald U, Waagepetersen HS, Schousboe A, He W, Lin JH, Han X, Takano T, Wang S, Sim FJ and others. 2007. The transcriptome and metabolic gene signature of protoplasmic astrocytes in the adult murine cortex. J Neurosci 27:12255-66.

Magistretti PJ, Pellerin L, Rothman DL, Shulman RG. 1999. Energy on demand. Science 283:496-7.

Martynoga B, Mateo JL, Zhou B, Andersen J, Achimastou A, Urban N, van den Berg D, Georgopoulou D, Hadjur S, Wittbrodt J and others. 2013. Epigenomic enhancer annotation reveals a key role for NFIX in neural stem cell quiescence. Genes Dev 27:1769-86.

McFarlane HG, Kusek GK, Yang M, Phoenix JL, Bolivar VJ, Crawley JN. 2008. Autism-like behavioral phenotypes in BTBR T+tf/J mice. Genes Brain Behav 7:152-63.

McKenna MC, Dienel GA, Sonnewald U, Waagepetersen HS, Schousboe A. 2012. Energy metabolism of the brain. In: Siegel G, Albers W, Brady S, Price D, editors. Basic neurochemistry. London: Elsevier. p 201-226.

Mira H, Andreu Z, Suh H, Lie DC, Jessberger S, Consiglio A, San Emeterio J, Hortiguela R, Marques-Torrejon MA, Nakashima K and others. 2010. Signaling through BMPR-IA regulates quiescence and long-term activity of neural stem cells in the adult hippocampus. Cell Stem Cell 7:78-89.

Monzon-Mayor M, Yanes C, Tholey G, De Barry J, Gombos G. 1990. Immunohistochemical localization of glutamine synthetase in mesencephalon and telencephalon of the lizard Gallotia galloti during ontogeny. Glia 3:81-97.

Parpura V, Heneka MT, Montana V, Oliet SH, Schousboe A, Haydon PG, Stout RF, Jr., Spray DC, Reichenbach A, Pannicke T and others. 2012. Glial cells in (patho)physiology. J Neurochem 121:4-27.

Pekny M, Leveen P, Pekna M, Eliasson C, Berthold CH, Westermark B, Betsholtz C. 1995. Mice lacking glial fibrillary acidic protein display astrocytes devoid of intermediate filaments but develop and reproduce normally. EMBO J 14:1590-8.

Perea G, Navarrete M, Araque A. 2009. Tripartite synapses: astrocytes process and control synaptic information. Trends Neurosci 32:421-31.

Robel S, Berninger B, Gotz M. 2011. The stem cell potential of glia: lessons from reactive gliosis. Nat Rev Neurosci 12:88-104.

Roybon L, Lamas NJ, Garcia-Diaz A, Yang EJ, Sattler R, Jackson-Lewis V, Kim YA, Kachel CA, Rothstein JD, Przedborski S and others. 2013. Human stem cell-derived spinal cord astrocytes with defined mature or reactive phenotypes. Cell Rep 4:1035-48.

Saura J. 2007. Microglial cells in astroglial cultures: a cautionary note. J Neuroinflammation 4:26.

Schildknecht S, Karreman C, Poltl D, Efremova L, Kullmann C, Gutbier S, Krug A, Scholz D, Gerding HR, Leist M. 2013. Generation of genetically-modified human differentiated cells for toxicological tests and the study of neurodegenerative diseases. ALTEX 30:427-44.

Schildknecht S, Pape R, Meiser J, Karreman C, Strittmatter T, Odermatt M, Cirri E, Friemel A, Ringwald M, Pasquarelli N and others. 2015. Preferential Extracellular Generation of the Active Parkinsonian Toxin MPP(+) by Transporter-Independent Export of the Intermediate MPDP(.). Antioxid Redox Signal 23:1001-16.

Schneider L. 2014. Survival of neural stem cells undergoing DNA damage-induced astrocytic differentiation in self-renewal-promoting conditions in vitro. PLoS One 9:e87228.

Schneider L, d'Adda di Fagagna F. 2012. Neural stem cells exposed to BrdU lose their global DNA methylation and undergo astrocytic differentiation. Nucleic Acids Res 40:5332-42.

Scholz D, Poltl D, Genewsky A, Weng M, Waldmann T, Schildknecht S, Leist M. 2011. Rapid, complete and large-scale generation of post-mitotic neurons from the human LUHMES cell line. J Neurochem 119:957-71.

Schousboe A, Bak LK, Waagepetersen HS. 2013. Astrocytic Control of Biosynthesis and Turnover of the Neurotransmitters Glutamate and GABA. Front Endocrinol (Lausanne) 4:102.

Sergent-Tanguy S, Michel DC, Neveu I, Naveilhan P. 2006. Long-lasting coexpression of nestin and glial fibrillary acidic protein in primary cultures of astroglial cells with a major participation of nestin(+)/GFAP(-) cells in cell proliferation. J Neurosci Res 83:1515-24.

Seri B, Garcia-Verdugo JM, McEwen BS, Alvarez-Buylla A. 2001. Astrocytes give rise to new neurons in the adult mammalian hippocampus. J Neurosci 21:7153-60.

Shaltouki A, Peng J, Liu Q, Rao MS, Zeng X. 2013. Efficient generation of astrocytes from human pluripotent stem cells in defined conditions. Stem Cells 31:941-52.

Shank RP, Bennett GS, Freytag SO, Campbell GL. 1985. Pyruvate carboxylase: an astrocyte-specific enzyme implicated in the replenishment of amino acid neurotransmitter pools. Brain Res 329:364-7.

Sirko S, Behrendt G, Johansson PA, Tripathi P, Costa M, Bek S, Heinrich C, Tiedt S, Colak D, Dichgans M and others. 2013. Reactive glia in the injured brain acquire stem cell properties in response to sonic hedgehog. [corrected]. Cell Stem Cell 12:426-39.

Smyth GK. 2004. Linear models and empirical bayes methods for assessing differential expression in microarray experiments. Statistical applications in genetics and molecular biology 3(1):1-25.

Sparmann A, Xie Y, Verhoeven E, Vermeulen M, Lancini C, Gargiulo G, Hulsman D, Mann M, Knoblich JA, van Lohuizen M. 2013. The chromodomain helicase Chd4 is required for Polycomb-mediated inhibition of astroglial differentiation. EMBO J 32:1598-612.

Stahlberg A, Andersson D, Aurelius J, Faiz M, Pekna M, Kubista M, Pekny M. 2011. Defining cell populations with single-cell gene expression profiling: correlations and identification of astrocyte subpopulations. Nucleic Acids Res 39:e24.

Steindler DA, Laywell ED. 2003. Astrocytes as stem cells: nomenclature, phenotype, and translation. Glia 43:62-9.

Su Z, Niu W, Liu ML, Zou Y, Zhang CL. 2014. In vivo conversion of astrocytes to neurons in the injured adult spinal cord. Nat Commun 5:3338.

Suarez I, Bodega G, Arilla E, Fernandez B. 1997. Region-selective glutamine synthetase expression in the rat central nervous system following portocaval anastomosis. Neuropathol Appl Neurobiol 23:254-61.

Sun Y, Pollard S, Conti L, Toselli M, Biella G, Parkin G, Willatt L, Falk A, Cattaneo E, Smith A. 2008. Long-term tripotent differentiation capacity of human neural stem (NS) cells in adherent culture. Mol Cell Neurosci 38:245-58.

Teslaa T, Teitell MA. 2015. Pluripotent stem cell energy metabolism: an update. EMBO J 34:138-53.

Ullensvang K, Lehre KP, Storm-Mathisen J, Danbolt NC. 1997. Differential developmental expression of the two rat brain glutamate transporter proteins GLAST and GLT. Eur J Neurosci 9:1646-55.

Volterra A, Meldolesi J. 2005. Astrocytes, from brain glue to communication elements: the revolution continues. Nat Rev Neurosci 6:626-40.

Waagepetersen HS, Bakken IJ, Larsson OM, Sonnewald U, Schousboe A. 1998. Comparison of lactate and glucose metabolism in cultured neocortical neurons and astrocytes using 13C-NMR spectroscopy. Dev Neurosci 20:310-20.

Waagepetersen HS, Sonnewald U, Schousboe A. 2009. Energy and amino acid neurotransmitter metabolism in astrocytes In: Parpura V, Haydon P, editors. Astrocytes in (patho)physiology of the nervous system Boston: Springer. p 177-200.

Walls AB, Bak LK, Sonnewald U, A. S, Waagepetersen HS. 2014. Metabolic mapping of astrocytes and neurons in culture using stable isotopes and gas chromatography-mass spectrometry (GC-MS). In: Hirlinger J, Waagepetersen HS, editors. Brain Energy Metabolism. New York: Springer. p 73-106.

Walz W, Lang MK. 1998. Immunocytochemical evidence for a distinct GFAP-negative subpopulation of astrocytes in the adult rat hippocampus. Neurosci Lett 257:127-30.

Wernig M, Meissner A, Foreman R, Brambrink T, Ku M, Hochedlinger K, Bernstein BE, Jaenisch R. 2007. In vitro reprogramming of fibroblasts into a pluripotent ES-cell-like state. Nature 448:318-24.

Westergaard N, Sonnewald U, Unsgard G, Peng L, Hertz L, Schousboe A. 1994. Uptake, release, and metabolism of citrate in neurons and astrocytes in primary cultures. J Neurochem 62:1727-33.

Wu Z, Irizarry RA, Gentleman R, Martinez-Murillo F, Spencer F. 2004. A model-based background adjustment for oligonucleotide expression arrays. J Amer Statist Assoc 99(468):909-917.

Zhou Y, Danbolt NC. 2013. GABA and Glutamate Transporters in Brain. Front Endocrinol (Lausanne) 4:165.

Zimmer B, Kuegler PB, Baudis B, Genewsky A, Tanavde V, Koh W, Tan B, Waldmann T, Kadereit S, Leist M. 2011a. Coordinated waves of gene expression during neuronal differentiation of embryonic stem cells as basis for novel approaches to developmental neurotoxicity testing. Cell Death Differ 18:383-95.

Zimmer B, Schildknecht S, Kuegler PB, Tanavde V, Kadereit S, Leist M. 2011b. Sensitivity of dopaminergic neuron differentiation from stem cells to chronic low-dose methylmercury exposure. Toxicol Sci 121:357-67.

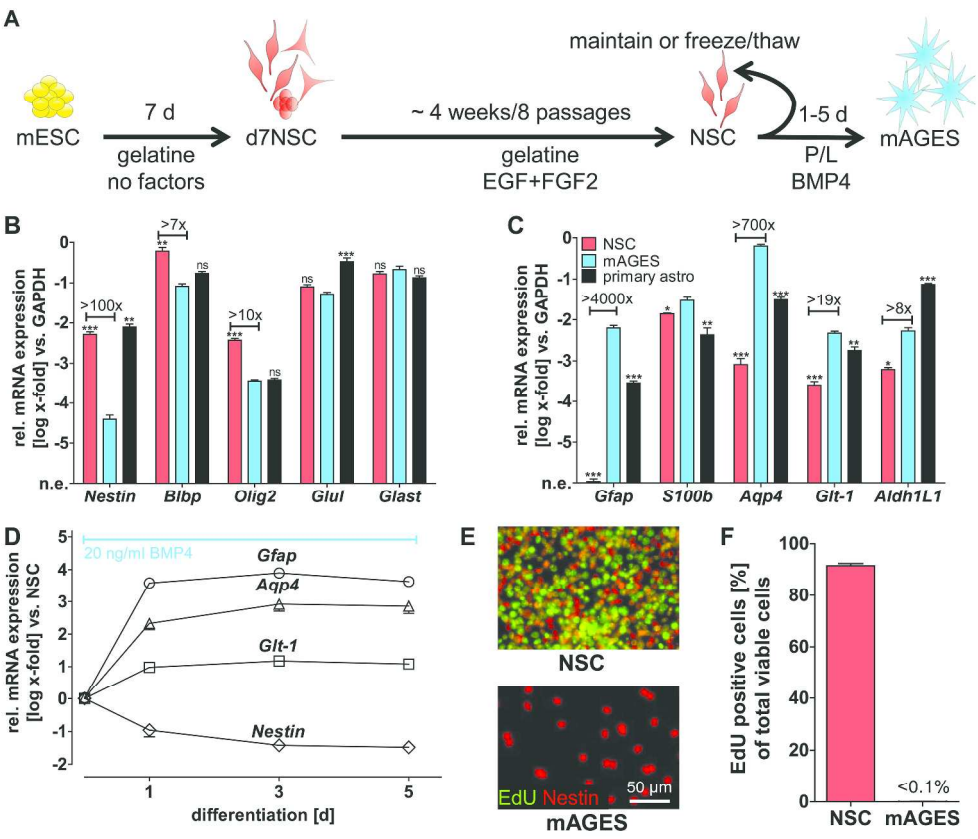

Figure 1. Kleiderman et al., 2015

583x513mm (250 x 250 DPI)

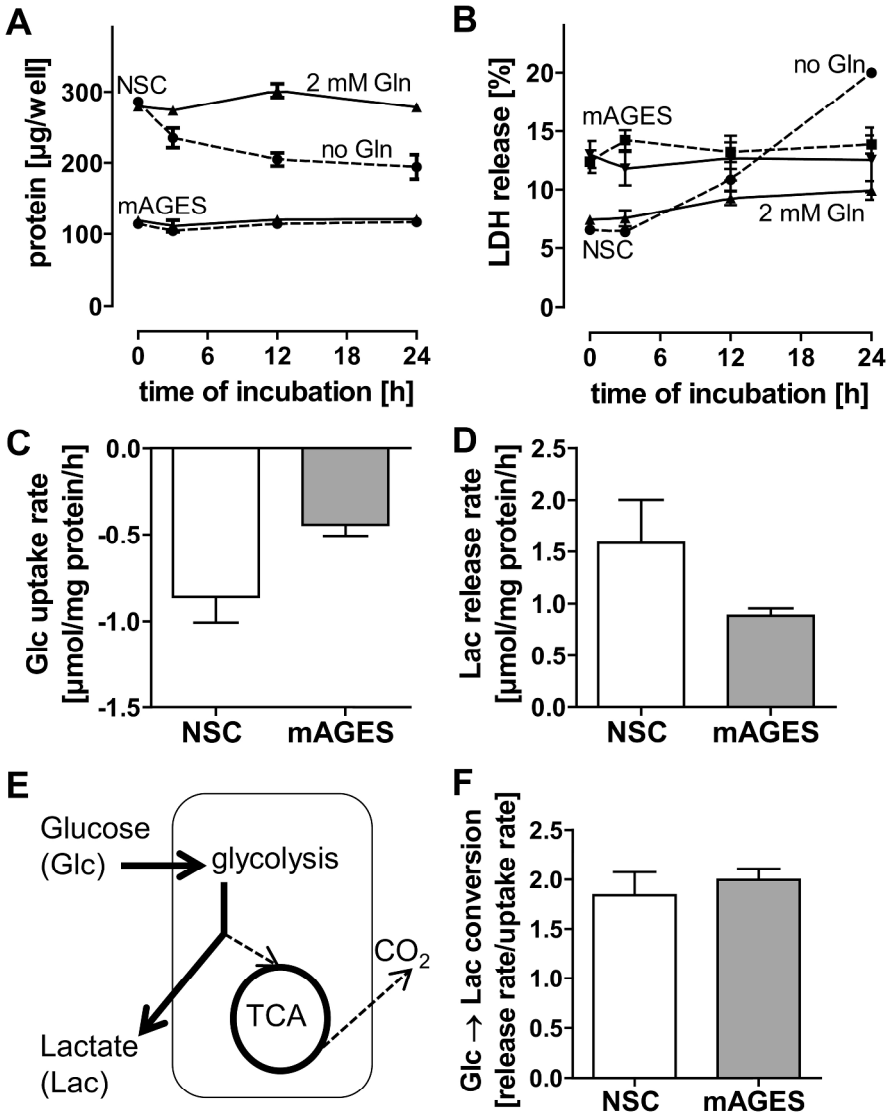

Figure 2. Kleiderman et al., 2015

140x175mm (600 x 600 DPI)

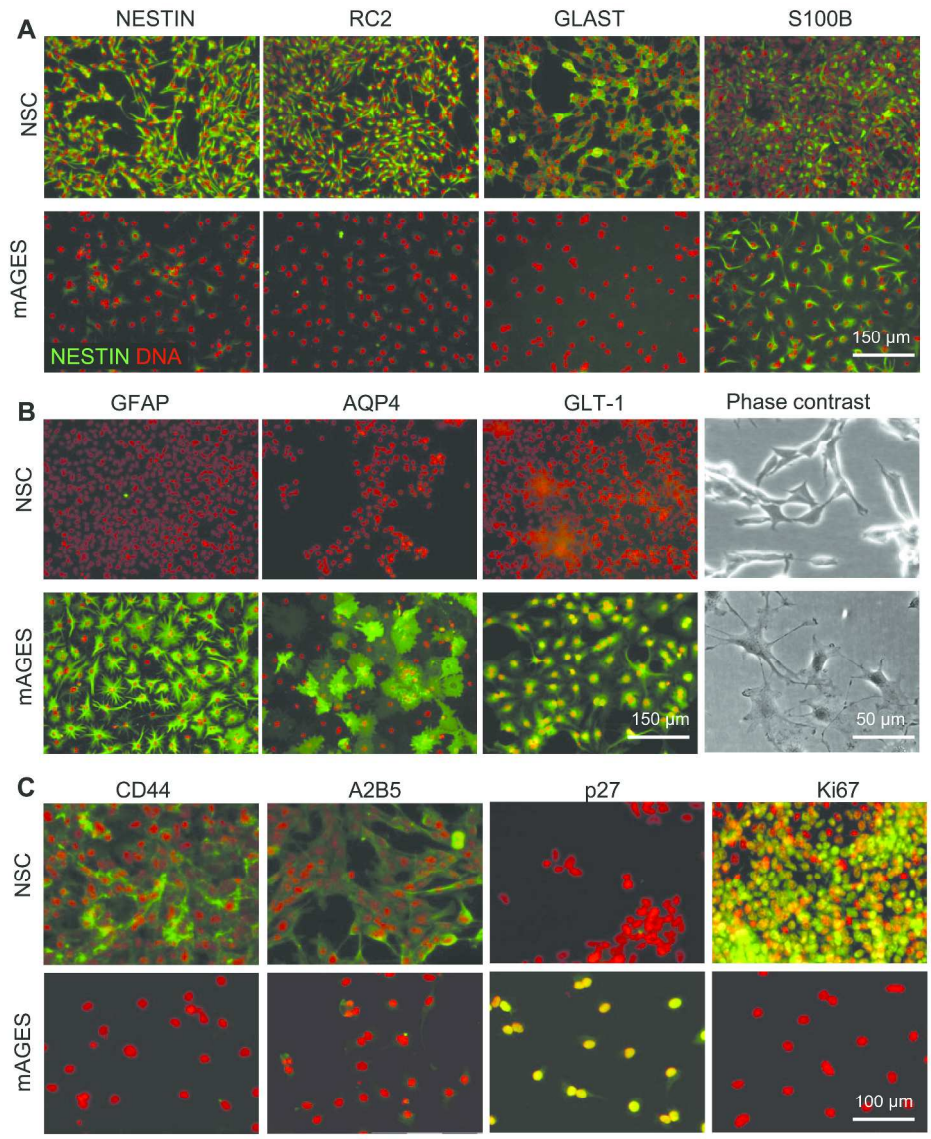

Figure 3. Kleiderman et al., 2015

194x244mm (600 x 600 DPI)

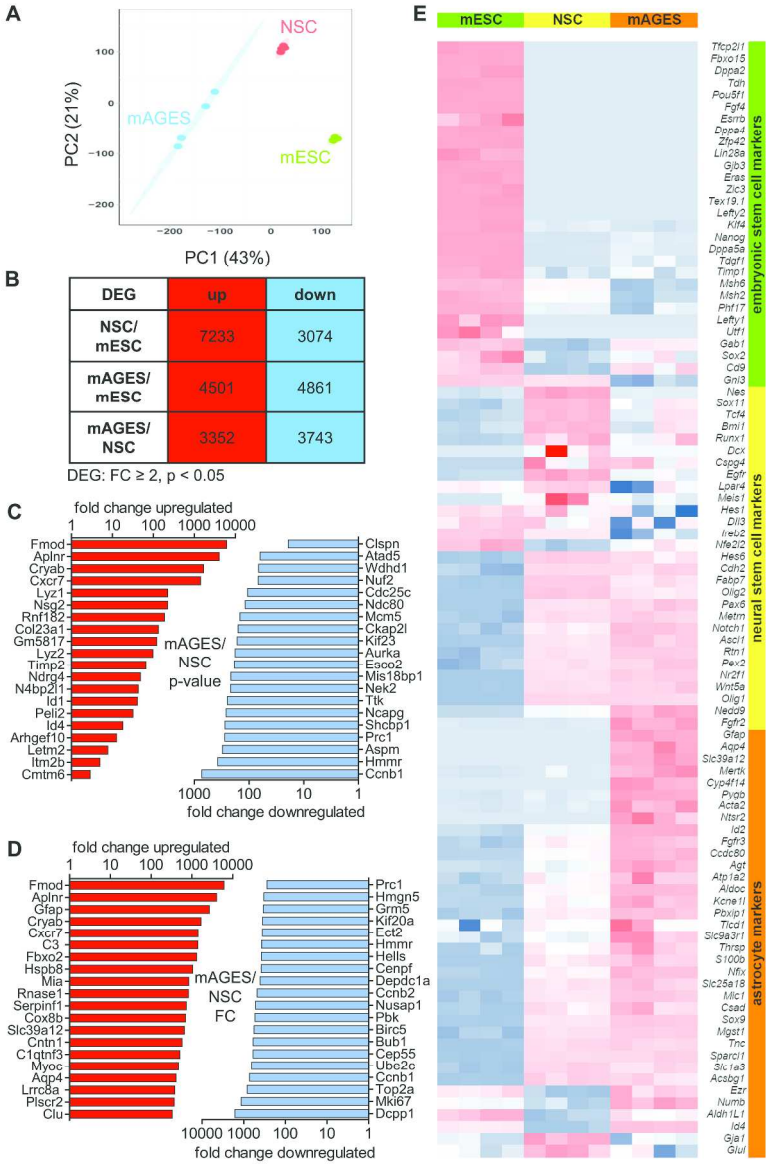

DEG	up	down
NSC/ mESC	7233	3074
mAGES/ mESC	4501	4861
mAGES/ NSC	3352	3743

Figure 4. Kleiderman et al., 2015

239x367mm (600 x 600 DPI)

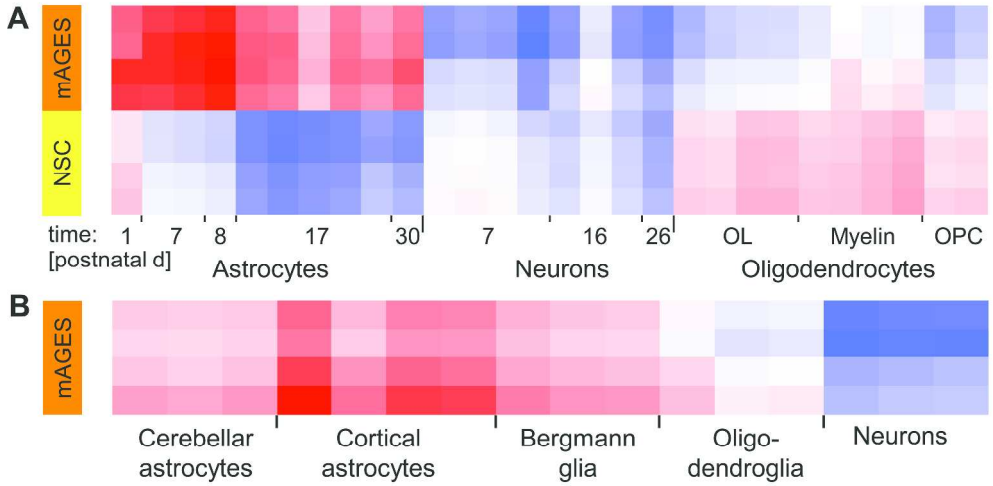

Figure 5. Kleiderman et al., 2015

560x303mm (300 x 300 DPI)

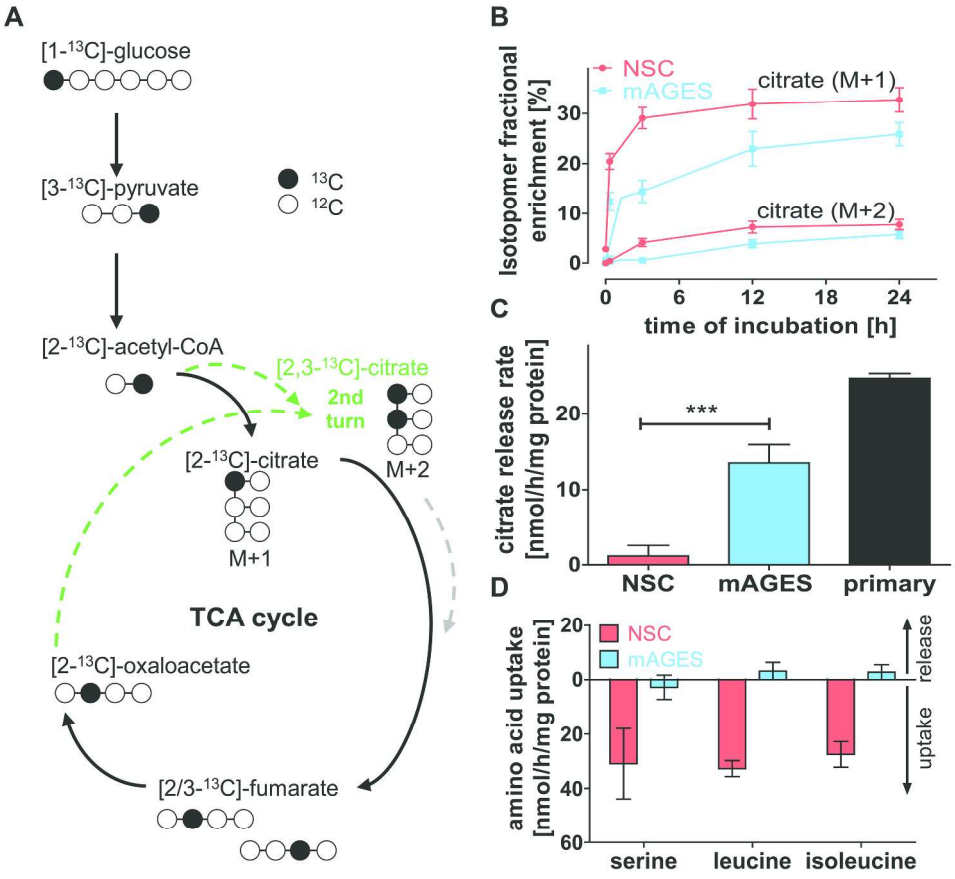

Figure 6. Kleiderman et al., 2015

146x135mm (600 x 600 DPI)

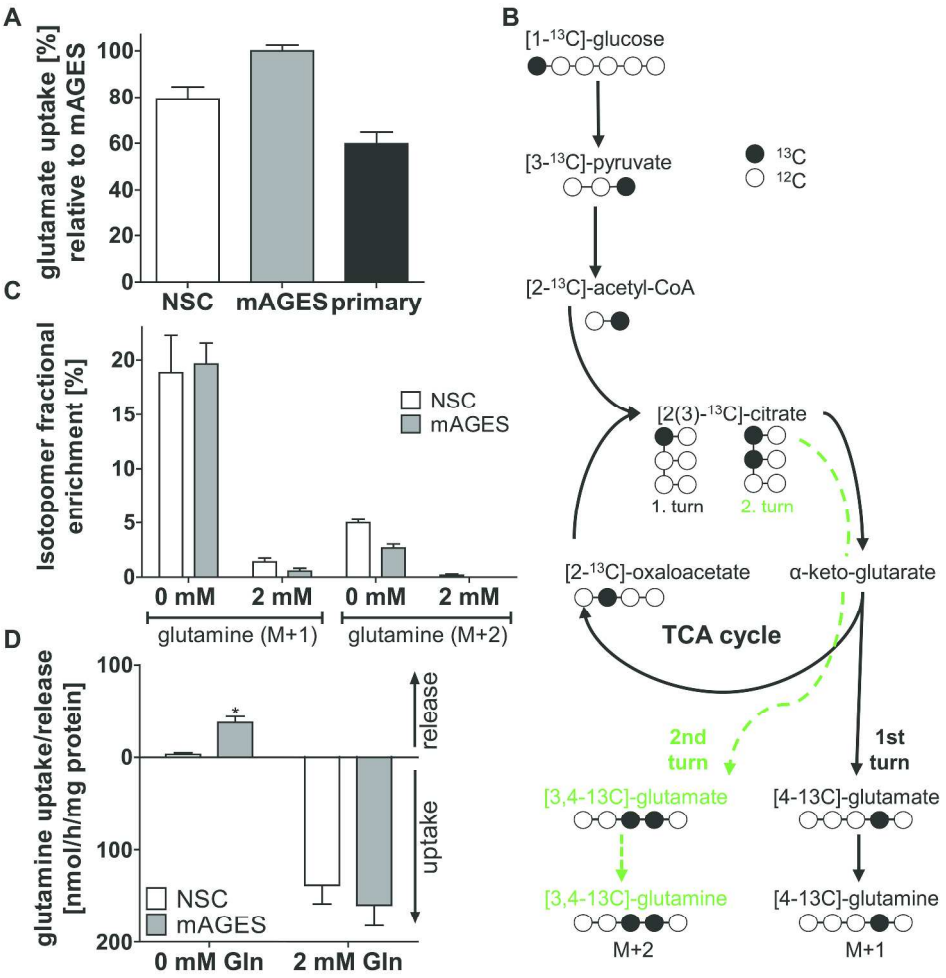

Figure 7. Kleiderman et al., 2015

172x175mm (600 x 600 DPI)

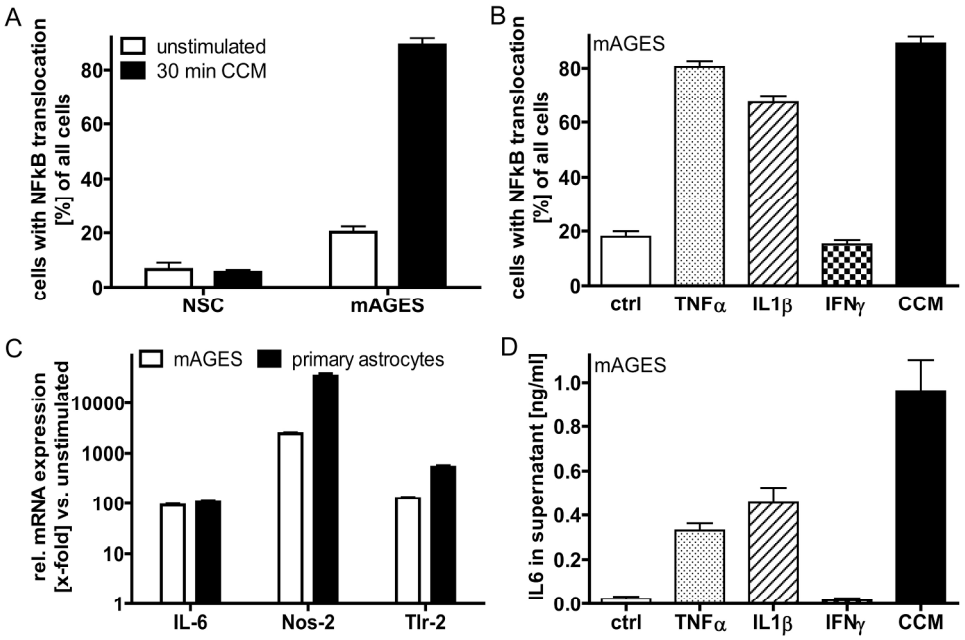

Figure 8. Kleiderman et al., 2015

117x82mm (600 x 600 DPI)

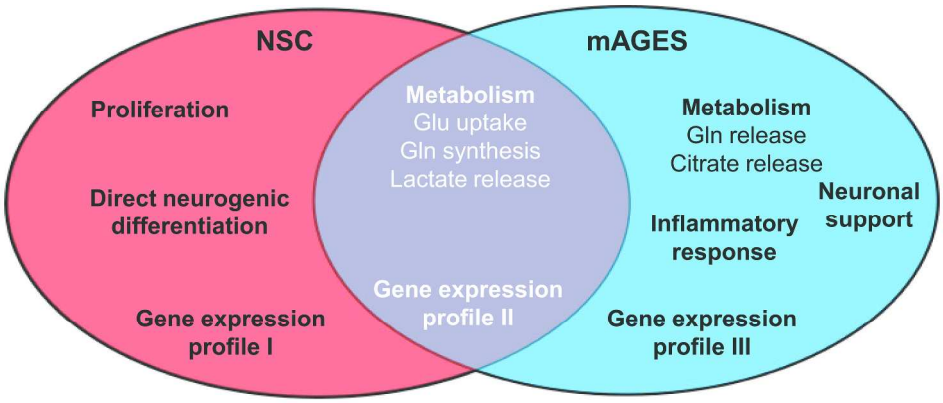

Gene expression profile								
I		II				III		
confirmed (diff. > 1.8)	new and validated	overlap, not specific				confirmed (diff. > 1.8)		new and validated	
Nes	*Ccnb1*	*Sox11*	*Pax6*	*Tlcd1*	*Acsbg1*	*Gfap*	*Ccdc80*	*Fmod*	*Nedd9**
Bmi1	*Hmmr*	*Tcf4*	*Metrn*	*Slc9a3r1*	*Ezr*	*Aqp4*	*Agt*	*Aplnr*	*Fgfr2**
Egfr	*Aspm*	*Runx1*	*Notch1*	*S100b*	*Numb*	*Slc39a12*	*Aldoc*	*Cryab*	
Ireb2	*Gja1**	*Lpar4*	*Ascl1*	*Slc25a18*	*Glul*	*Mertk*	*Kcne1l*	*Cxcr7*	
Fabp7		*Meis1*	*Rtn1*	*Csad*		*Cyp4f14*	*Pbxip1*	*Lyz1/2*	
Olig2		*Hes1*	*Pex2*	*Sox9*		*Pygb*	*Thrsp*	*Nsg2*	
		Dll3	*Nr2f1*	*Mgst1*		*Acta2*	*Nfix*	*Rnf182*	
		Nfe2l2	*Wnt5a*	*Tnc*		*Ntsr2*	*Mlc1*	*Col23a1*	
		Hes6	*Olig1*	*Sparcl1*		*Id2*	*Aldh1L1*	*Timp2*	
		Cdh2	*Atp1a2*	*Slc1a3*		*Fgfr3*	*Id4*	*Ndrg4*	

Figure 9. Kleiderman et al., 2015

151x128mm (600 x 600 DPI)

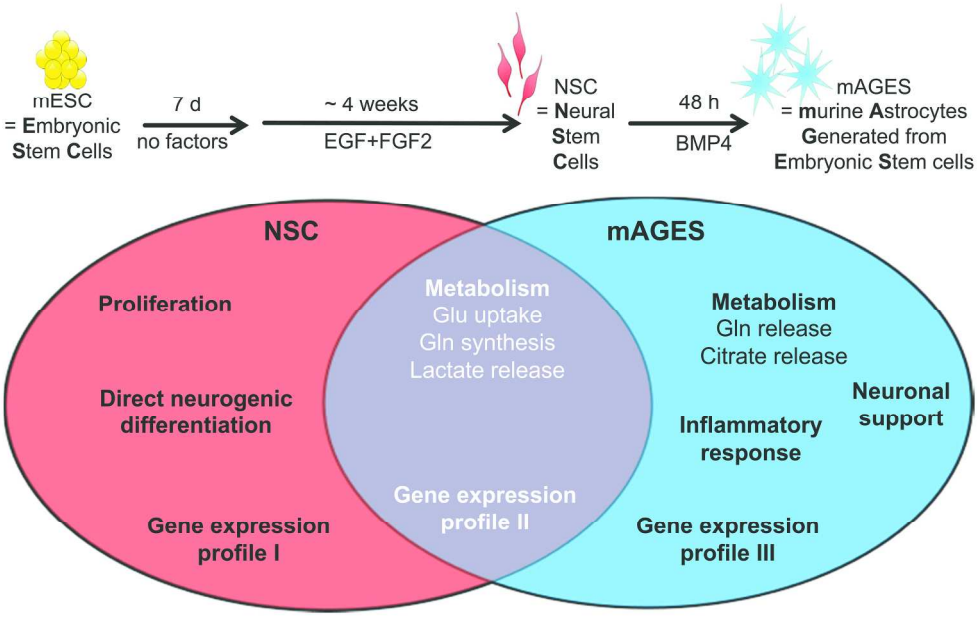

117x74mm (600 x 600 DPI)

SUPPLEMENTAL MATERIAL

Pure populations of stem cell-derived mature astrocytes reveal differences in metabolism and inflammatory response during development

Susanne Kleiderman , João A. Sá, Ana P. Teixeira, Catarina Brito, Simon Gutbier, Lars G. Evje, Mussie G. Hadera, Enrico Glaab, Margit Henry, Sachinidis Agapios, Paula M. Alves, Ursula Sonnewald, and Marcel Leist.

Glia

Table of Contents

A. Supplemental methods

LUHMES co-culture and neurite area measurement

NSC were seeded at different cell densities on poly-ornithin/laminin-coated plates and differentiated for 3 days with 20 ng/ml BMP4 to mAGES. LUHMES were maintained and differentiated for neurite outgrowth measurements as described before (Krug et al. 2013a). In brief, LUHMES were replated in proliferation medium. After 24 h, medium was changed to differentiation medium for 2 days to pre-differentiate LUHMES. Pre-differentiated LUHMES were trypsinized, counted, and plated on top of 3-days old mAGES at a density of 150,000 cells/cm^2 in LUHMES differentiation medium containing GDNF, cAMP, and tetracycline. Medium was changed once after 2 days and cells were maintained for further 10 days without medium exchange. For analysis, cells were fixed and stained for βIII Tubulin (TUJ1) (LUHMES) and GFAP (mAGES). For neurite area measurement, GFP-overexpressing LUHMES were used. Nuclei were stained with H-33342 to detect valid cells and GFP was used as a measure for neurite area using the spot detector algorithm.

B. Supplemental material

1. Cell culture material	Cat. No.	Provider
β-mercaptoethanol	1350	Gibco
Adv. DMEM/F-12 w/o Glc	RR14026.01	Fisher Scientific
B27-supplement	17504	Gibco
Bone morphogenetic protein (BMP4)	314-BP	R&D Systems
Bovine serum albumin (BSA)	K41-001	GE Healthcare
D-Glucose-1-13C	297046	Sigma
DMEM/F-12	21331	Gibco
Fetal bovine serum (FBS)	A15-101	PAA(GE Healthcare)
Gelatine from porcine skin	G1890	Sigma
Glutamax	35050	Gibco
GMEM	21710	Gibco
Insulin solution human	I9278	Sigma
Laminin	L2020	Sigma
Leukemia inhibitory factor (LIF)	ESG1106	Millipore
N2 supplement	17502	Gibco
Neurobasal medium	21103	Gibco
Neurobasal-A w/o Glc	A24775-01	Gibco
Non-essential amino acids	1140	Gibco
Poly-L-ornithine hydrobromide	P3655	Sigma
Recombinant human FGF basic	233-FB	R&D Systems
Recombinant human EGF	236-EG	R&D Systems
Sodium pyruvate	11360	Gibco
Trypsin-EDTA	25300062	Gibco

2. Primers

Name	Accession	Forward sequence	Reverse sequence
Aldh1l1	NM_027406.1	5’-CTCGGTTTGCTGATGGGGACG-3’	5’ GCTTGAATCCTCCAAAAGGTGCGG-3’
Aplnr	NM_011784.3	5’-GGGAGTAAGTTTGGGAAAGAG-3’	5’-TGGAATATGTCTTGTCCTTGG-3’
Aqp4	NM_009700.2	5’-GCTCAGAAAACCCCTTACCTGTGG-3’	5’-TTCCATGAACCGTGGTGACTCC-3’
Aspm	NM_009791.4	5’-GCCTCTCTCGGCCTCCATCAGCCTCCTTG-3’	5’-AGGCAGCGTTGCTTCTATCAACAGCGTCG-3’
Blbp	NM_021272.3	5’-GGGTAAGACCCGAGTTCCTC-3’	5’-ATCACCACTTTGCCACCTTC-3’

Ccnb1	NM_172301.3	5’-GGGTGTGCTTTGAATTCTGACA-3’	5’-AGGAGTGGCGCCTTGGTAT-3’
Col23a1	NM_153393.2	5’-GACCTGGAGAACCAGGACTCGATG-3’	5’-CATCCAAACGGATCTGTACAGGTC-3’
Cryab	NM_009964.3	5’-CGGACTCTCAGAGATGCGTT-3’	5’-TGGGATCCGGTACTTCCTGT-3’
Cxcr7	NM_007722.4	5’-GAGGTCACTTGGTCGCTCTC-3’	5’-GTGTCCACCACAATGCAGTC-3’
Fmod	NM_021355.3	5’-GAAGGGTTGTTACGCAAATGG-3’	5’-AGATCACCCCCTAGTCTGGGTTA-3’
Gfap	NM_010277.3	5’-GCCCGGCTCGAGGTCGAG-3’	5’-GTCTATACGCAGCCAGGTTGTTCTCT-3’
Glast	NM_148938.3	5’-CTCTACGAGGCTTTGGCTGC-3’	5’-GAGGCGGTCCAGAAACCAGTC-3’
Glt-1	NM_010927.3	5’-GCAGCCATCTTCATAGCCCAAATG-3’	5’-CTCATTCTATCCAGCAGCCAGTCC-3’
Glul	NM_008131.4	5’-GTGTGTGGAAGAGTTACCTGAGTGG-3’	5’-ATGTGCCTCAAGTTGGTCTCTGC-3’
Hmmr	NM_013552.2	5’-GGCATTGTTGAATGAACATGGTGCA-3’	5’-TGTTTCCTTTTAACAAGCTGAGATCGGAGT-3’
IL-6	NM_031168.1	5’-CCTCTGGTCTTCTGGAGTACCATAGC-3’	5’-GGAGAGCATTGGAAATTGGGGTAGG-3’
Lyz1/2	NM_017372.3	5’-TGACATCACTGCAGCCATAC-3’	5’-TGGGACAGATCTCGGTTTTG-3’
Ndrg4	NM_145602.3	5’-AAGTACGTGATTGGCATTGGAGT-3’	5’-CAGGTGCATTATCTCCGACTACC-3’
Nestin	NM_016701.3	5’-CTGGAAGGTGGGCAGCAACT-3’	5’-ATTAGGCAAGGGGGAAGAGAAGGTG-3’
Nos-2	NM_010927.3	5’-TTGCCACGGACGAGACGGATAGG-3’	5’-GGGGTTGTTGCTGAACTTCCAGTC-3’
Nsg2	NM_008741.4	5’-AGACCGTCCCTCTCATCACG-3’	5’-TCTGTTCCGGCTGGTATTCTG-3’
Olig2	NM_016967.2	5’-GGCGGTGGCTTCAAGTCATC-3’	5’-TAGTTTCGCGCCAGCAGCAG-3’
Prom1	NM_008935.2	5’-TGAAGAAGATCCTTGCCTC-3’	5’-TCCGCAACATAGCCACAC-3’
Rnf182	NM_183204.4	5’-AGCCTGCCCGATGACAAC-3’	5’-CTTCCCTTTGCCTCCACAAG-3’
S100b	NM_009115.3	5’-GGTTGCCCTCATTGATGTCTTCCAC-3’	5’-CTTCCTGCTCCTTGATTTCCTCCAG-3’
Timp2	NM_011594.3	5’-AGACGTAGTGATCAGGGCCA-3’	5’-GTACCACGCGCAAGAACCAT-3’
Tlr-2	NM_011905.3	5’-CCTCCGTCTTGGAATGTCACCAGG-3’	5’-GAGCCACGCCCACATCATTC-3’

3. Antibodies	**Dilution**	**Cat. No.**	**Provider**
A2B5	1:200	A8229	Sigma
AQP4	1:500	sc-20812	Santa Cruz
CD133/prominin 1	1:200	14-1331	eBioscience
CD44	1:500	RM5704	Caltag Lab
GFAP	1:1000	556330	BD Pharmingen
GLAST	1:200	130-095-822	Miltenyi Biotec
GLT-1	1:200	AB1783	Millipore
Nestin	1:500	MAB353	Millipore
NeuN	1:200	MAB377	Millipore
NFkB p65	1:200	sc-372	Santa Cruz
PSD95	1:500	sc-28941	Santa Cruz
RC2	1:100	ID: AB_531887	DSHB
S100B	1:1000	52532	Sigma
Synapsin	1:500	106 001	Synaptic System
TUJ1	1:1000	MMS-435-250	Covance

C. Supplemental figures

Supplemental figure S1. Selection of the desired cell populations from fresh NSC cultures and increasing capacity to generate mAGES over passage number.
(A) NSC from different passage numbers were exposed to 20 ng/ml BMP4 for 3 days to trigger differentiation to mAGES. The upper row shows exemplary pictures (immunocytochemistry for GFAP- (green) and AQP4-positive (red) cells) indicating the differential success of differentiation. The lower row shows the residual nestin expression (green). DNA was counterstained with Hoechst H-33342 (blue). The mAGES from passage 10 still showed some nestin-positive cells, but with significantly lower intensity per cell than in earlier passages. **(B)** Phase contrast pictures of NSC at different passage numbers were taken from live cells. At passage 2, the population consisted of cells, which differed in their morphology and attachment behavior. Some fast growing cells were forming clumps (type I). Some slow growing triangular cells (type II) were more adherent than bipolar NSC (type III). At passage 9 – 12 (with continued selection for type III cells), the NSC population was homogeneous and contained mainly the desired bipolar type of NSC. The different cell types from passage 2 are displayed at higher magnification for clarification.

Supplemental figure S2. Selection of homogeneous NSC from the fresh/early passage mixed NSC culture.
Phase contrast pictures were obtained from NSC at passage 2. Three couples of pictures illustrate cultures before and after the indicated manipulations designed to enrich for the desired NSC population. (**A**) Tapping the plate several times removed aggregating type I cells (see supplemental figure S1A), which were only loosely attached to the surface coating or to other cells. (**B**) Scraping of cell clumps, which were visible to the unaided eye, with an aspiration plastic pipette removed aggregating type I cells, which were not removed by tapping the flask. (**C**) Cells were treated with 0.05% trypsin for 10 s, and cell culture flasks were washed once with medium. Pictures before and after trypsinization revealed that the flat, triangular type II cells (see supplemental figure S1A) did not detach from the coated surface within this time period of treatment (red border). The desired bipolar type III NSC (green border) were harvested from the trypsin solution, and were further expanded.

Supplemental figure S3. Immunocytochemical characterization of fresh NSC vs homogeneous NSC at higher passage numbers.
NSC were fixed and permeabilized at different passage numbers. Examples from passage 2 (early, heterogeneous) and passage 12 (late, homogeneous) are shown. Nestin (**A**) or RC2 (**B**) expression (green) were visualized by immunocytochemistry. DNA was counterstained with Hoechst H-33342 (red). (**A**) The aggregating type I cells (see supplemental figure S1A) in NSC of passage number 2 did not express nestin. The triangular type II cells showed moderate nestin expression. The bipolar type II NSC highly expressed nestin. (**B**) The aggregating type I cells in NSC of passage number 2 did not express detectable levels of RC2, and the triangular type II cells expressed moderate RC2. Only the bipolar type II NSC highly expressed RC2.

Supplemental figure S4. NSC are multipotent neural stem cells producing neurons.
(**A**) NSC (at passage number > 10) were replated on poly-ornithin/laminin-coated plates in N2B27 medium without EGF and with 10 ng/ml FGF2 at a density of 30,000 cells/cm^2. On day 2, the FGF2 concentration was reduced to 5 ng/ml. On day 4, N2B27 medium was added without growth factors. After 14 days, most of the NSC differentiated into neurons. (**B**) NSC were differentiated into neurons as described in A and on day 14, cells were fixed and stained for βIII-Tubulin (TUJ1, red), nestin or GFAP (green) and nuclei were counterstained with H-33342 (blue). (**C**) NSC were differentiated and stained as described in B and TUJ1, GFAP, or nestin-positive cells were counted. While most of the cells differentiated into TUJ1-positive neurons (60%), 30% produced GFAP-positive astrocytes. Many cells expressed nestin, either with or without co-expression of GFAP and TUJ1. (**D**) NSC were differentiated as described in A. On day 21, cells were fixed and stained for TUJ1 (red) and NeuN (green) and counterstained with H-33342 (blue). Expression of the neuronal marker NeuN in the nuclei of TUJ1-positive neurons confirmed their maturity.

Supplemental figure S5. Single cell cloning reveals homogeneity of the NSC population and multipotency of single NSC.
NSC were plated at clonal density in EGF/FGF2-containing medium on gelatin-coated 96 well plates and clones were expanded for several passages. (**A,B**) The different NSC clones were differentiated for 3 days in 20 ng/ml BMP4-containing medium to obtain mAGES. Cells were fixed and stained for GFAP (green) and DNA was counterstained with H-33342 (blue). GFAP-positive cells were counted (B). (**C,D**) The different NSC clones were differentiated for 14 days as in supplemental figure S4A. Cells were fixed and stained for βIII- Tubulin (TUJ1, red), GFAP (green) and DNA was counterstained with H-33342 (blue). TUJ1- and GFAP-positive cells were counted (D).

Supplemental figure S6. Differentiation of mAGES from different mESC lines of distinct genetic backgrounds.
(**A**) NSC were differentiated from different mESC lines DO335.45, BTBR, and O9 iPS cells. NSC were further differentiated to mAGES with 20 ng/ml BMP4 for 3 days. GFAP, AQP4, and nestin are visualized by immunocytochemistry (green). Nuclei were counterstained with H-33342 (red). Almost all cells expressed GFAP, although they slightly differed in their morphology. AQP4 was expressed by more than 50% of the cells, while nestin was strongly downregulated in all cells. (**B**) Five days old mAGES from DO335.45, BTBR, and iPS were exposed to complete cytokine mix (CCM), 10 ng/ml TNFα, and 20 ng/ml IFNγ for 30 min. Cells were fixed, permeabilized, and NFkB was visualized by immunocytochemistry. Nuclei were counterstained with H-33342. The ratio of NFkB in the cytosol and the nucleus was measured in NSC and mAGES cultures by an automated screening microscope (1,000 nuclei/condition). The number of cells with NFkB translocation into nuclei in percent of total viable cells (apoptotic nuclei are excluded) was calculated relative to unstimulated cells using the nuclear translocation algorithm. All mAGES showed the same response pattern as the CGR8.0-mAGES control line; they responded to TNFα, but not to IFNγ. Data are means ± SEM from triplicate determination of three independent experiments.

Supplemental figure 7. Different phenotypes and proliferation behavior of mAGES differentiated from NSC with BMP4, FBS, or LIF.

(**A**,**B**) NSC were differentiated to mAGES for 3 days with 20 ng/ml BMP4, 2-10 % FBS, or 1,000 U/ml LIF. GFAP (**A**) or nestin (**B**) were visualized by immunocytochemistry (nuclei were counterstained with H-33342) and percentage of positive cells was measured with the high throughput device CellInsight™ CX5 using the target activation algorithm (1,000 cells/condition). All factors induced GFAP expression, although BMP4 revealed best induction. Nestin was only downregulated with BMP4 and FBS, although BMP4 revealed higher downregulation. LIF was not sufficient to downregulate nestin. CNTF exposure resulted in the same phenotype as LIF (not shown) (**C**) NSC and mAGES (3 days old) were incubated with the nucleoside analogue EdU (10 μM) for 48 h, before cells were fixed. Then, EdU incorporation was visualized by immunocytochemistry, and nuclei were counterstained with H-33342. The number of nuclei that were EdU-positive was counted in NSC and mAGES cultures by an automated screening microscope (1,000 nuclei/condition). EdU incorporation was not detected in BMP4-differentiated control mAGES. However, some cells differentiated with FBS were still proliferating (1-3%), although proliferation decreased with increasing FBS concentration. LIF was not sufficient to induce cell cycle exit of mAGES. LIF, together with BMP4, induced cell cycle exit. Only BMP4 was sufficient to differentiate NSC into fully mature, non-proliferating mAGES. (**D**) Immunofluorescent pictures of GFAP and nestin, which were counted in (A,B), show that only BMP4 induces a star-shaped morphology of mAGES. Data are means ± SEM from triplicate determination of three independent experiments, *$p < 0.05$.

Supplemental figure S8. Inhibition of astrocytogenesis by valproic acid (VPA).

(**A**) NSC were differentiated to mAGES with 20 ng/ml BMP4 in the presence of VPA for 48 h. Cells were fixed, permeabilized, and GFAP, Aqp4, and nestin were visualized by immunocytochemistry and nuclei were counterstained with H-33342. The number of positive cells was counted in mAGES cultures by an automated screening microscope (1,000 cells/condition). VPA significantly inhibited differentiation as indicated by a lack of GFAP- and AQP4-upregulation and nestin-downregulation. While VPA did not influence viability of mature astrocytes within 48 h measured by resazurin reduction, a reduction of viability was seen at 10 mM in differentiating cells (not shown). (**B**) NSC were differentiated to mAGES with 20 ng/ml BMP4 for 72 h and exposed to VPA within the first 24 h of differentiation. Cells were washed 3 times after 24 h to remove VPA. Measurement of positive cells was performed as in (A). VPA still significantly and sustainably inhibited differentiation of NSC to mAGES. Data are means ± SEM from triplicate determination of three independent experiments. ***$p < 0.0001$ (Oneway ANOVA with Dunnett's post test).

Supplemental figure S9. Display of the top 20 differentially expressed genes in NSC relative to mESC.
RNA was prepared from 4 independent differentiations of NSC and mAGES (5 days old) and used for Affymetrix Mouse Genome 430 2.0 Arrays. Differentially expressed genes in NSC vs mESC were determined using the Empirical Bayes moderated t-statistic and adjusted for multiple hypothesis testing using the Benjamini-Hochberg method. A false-discovery rate threshold of 0.05 was chosen to determine the sets of significantly differential genes. The gene list was sorted by adjusted p-value and the top 20 differentially expressed genes in NSC relative to mESC were selected. Bars indicate fold change of genes, which were upregulated (red) or downregulated (blue) in NSC relative to mESC.

Supplemental figure S10. The top 20 differentially expressed genes in NSC, mAGES, and mESC.
The top 20 DEG in mAGES relative to NSC (**A,B,C,D**) or NSC relative to mESC (**E,F**) depicted in figure 4C,D and supplemental figure S9 are listed giving the logarithmized (to the base of 2) mean absolute expression values.

Supplemental figure S11. The mean absolute expression values [log_2] of 94 selected cell type specific genes shown in the heatmap of Fig. 4.

Supplemental figure S12. Validation of DEG with qPCR.
(**A,C**) For measurements of gene expression by qPCR, mRNA was prepared from mAGES (after 5 days of differentiation) or NSC. All data are given in fold difference (x-fold) relative to the housekeeping gene *Gapdh*. (**B,D**) Data from A are given relative to the expression in NSC (B) or relative to mAGES (D), based on the ΔΔCT method (note logarithmic axis scaling). Data are means ± SEM from three experiments.

Supplemental figure S13. Comparison of the top 20 DEG to *in vivo* data.
Micorarray analysis by Beckervordersandforth et al. 2010 for non-neurogenic, parenchymal astrocytes (astrocytes) from the diencephalon and adult neural stem cells (aNSC) from the SVZ was monitored for the expression of the top 20 upregulated genes (**A**) and the top 20 downregulated genes (**B**) found in mAGES relative to NSC. Expression is depicted as mean absolute expression values (from 4 replicates respectively). Data are means ± SEM.

Supplemental figure S14. 1H-NMR spectra of citrate in supernatants of NSC and mAGES.
Cells (mAGES/NSC) were plated in 6 well plates at a density of 500,000 cells/well for mAGES and 80,000 cells/well for NSC. After 48 h (5 days for mAGES), medium was changed to glucose-free medium supplemented with 10 mM D-[1-13C]-glucose with either 2 mM glutamine (Gln) or no Gln. Supernatants were harvested after indicated time points. Citrate was measured in supernatants of NSC and mAGES using 1H-NMR spectroscopy and spectra are depicted together with citrate spikes in black.

Supplemental figure S15. Neuronal support by mAGES.
NSC were differentiated for 3 days with 20 ng/ml BMP4 at different initial cell densities to obtain mAGES. Then, LUHMES were plated on top of mAGES in LUHMES differentiation medium at

a density of 150,000 cells/cm^2. Two days later, medium was changed and cells were maintained for 10 days without medium exchange. (**A**) 30,000 mAGES per well were co-cultured for 12 days with LUHMES. Cells were fixed and stained for βIII tubulin (TUJ1) and GFAP. Nuclei were counterstained with H-33342. The mAGES obtained an extreme star-shaped morphology morphology when co-cultured with LUHMES. (**B**) 150,000 LUHMES were cultured either alone or in co-culture with 30,000 mAGES for 6 or 14 days. Cells were fixed and stained for βIII tubulin (TUJ1), and nuclei were counterstained with H-33342. In co-culture, LUHMES still formed a dense neurite network at day 14 in the presence of mAGES. (**C**) GFP-overexpressing LUHMES were plated on top of mAGES or NSC at different cell densities. On day 6 or 14 of LUHMES differentiation, neurite area was measured using an established algorithm on an automated screening microscope. Only mAGES supported LUHMES survival within the culture period. LUHMES alone or in co-culture with NSC died.

Supplemental figure S16. Enhancement of synaptogenesis in LUHMES by mAGES.
NSC were seeded at an initial density of 20,000 cells/cm^2 and cultured for 2 days in medium containing EGF/FGF2 or seeded at 50,000 cells/cm^2 and differentiated for 3 days with 20 ng/ml BMP4 to obtain mAGES. Then, cells were washed once with PBS and LUHMES were plated on top of NSC or mAGES in LUHMES differentiation medium at a (low) density of 15,000 cells/cm^2. For comparison, LUHMES control cultures were prepared (white bars, 15,000 cells/cm^2, poly-ornithin/fibronectin-coating, no other cells). Four days later, cells were fixed, permeabilized and immunostained for the neuronal marker βIII- Tubulin (TUJ1), the postsynaptic marker PSD95, and the presynaptic marker synapsin 1. DNA was counterstained with H-33342. Postynaptic puncta labeled by PSD95 (**A**) or presynaptic puncta labeled by synapsin 1 (**B**) on neurites (TUJ1) of LUHMES alone or in co-culture with NSC or mAGES were counted using an established algorithm (neuronal profiling) on an automated screening microscope. (**C**) Overlapping puncta of PSD95 and synapsin 1 were automatically counted as described in A. LUHMES alone (**D**) or in co-culture with mAGES (**E**) were analyzed by confocal imaging. Representative images of PSD95 and synapsin 1 puncta on TUJ1-labeled neurites have been chosen.

Supplemental figure S17. NFkB translocation in mAGES and NSC after cytokine stimulation.
(A) NSC and 5 days old mAGES were exposed to complete cytokine mix (CCM, 10 ng/ml TNFα, 10 ng/ml IL1β, and 20 ng/ml IFNγ) for 30 min. Then, cells were fixed, permeabilized, and immunostained for the p65 unit of the inflammatory transcription factor NF-κB (NFkB, green). Nuclei were counterstained with H-33342 (red). In unstimulated cells, NFkB was distributed throughout the cytosol. Upon CCM-stimulation, NFkB was translocated to the nucleus only in mAGES, not in NSC, revealed by an overlap of H-33342 and NFkB (yellow nuclei). Some mAGES were not reactive, showing no NFkB translocation from the cytosol to the nucleus (red nuclei). Cells were counted and the percentage of activated cells is shown below the pictures.

Supplemental figure S18. mAGES are not quiescent stem cells.
(**A**) NSC were differentiated for 3 days with 20 ng/ml BMP4 either with or without 20 ng/ml FGF2 to obtain mAGES. Cells were exposed to 10 μM EdU for 48 h. Then, cells were fixed and immunostained for GFAP, nestin, and EdU. The mAGES adopted a star-shaped morphology,

even in the presence of FGF2 during differentiation, but they resembled reactive astrocytes (more feathery morphology). The cells did not incorporate EdU into DNA within 48 h of incubation. (**B**) Cells were differentiated and stained as in A and positive cells were counted. While all cells upregulated GFAP in both conditions, the amount of nestin-expressing cells was higher, when FGF2 was present during differentiation. Data are means ± SEM from three experiments. * $p < 0.05$ (**C**) For measurements of gene expression by qPCR, mRNA was prepared from mAGES (after 3 days of differentiation), NSC of passage 12 (p12), or freshly prepared NSC from passage 2 (p2). The expression of the (quiescent) stem cell marker CD133/prominin1 mRNA is given in fold difference (x-fold) relative to the housekeeping gene *Gapdh* (note logarithmic axis scaling). The expression of CD133 in mAGES and NSC cultures was below the detection limit (35 cycles, n.e. not expressed). (**D**) NSC at passage 2, NSC (passage 12), and 3 days old mAGES were fixed (no permeabilization) and immunostained for the (quiescent) stem cell marker CD133/Prominin1.

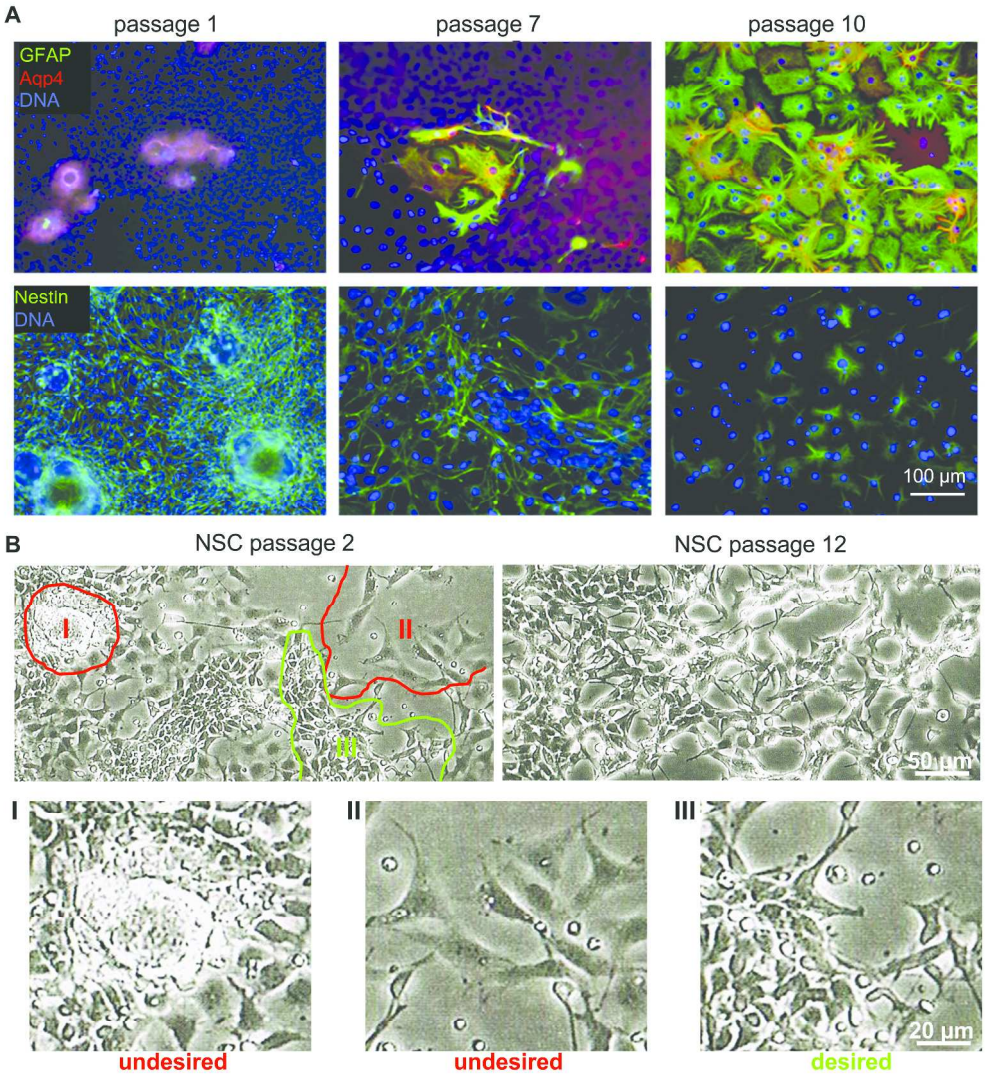

Supplemental figure S1. Kleiderman et al. 2015

211x241mm (600 x 600 DPI)

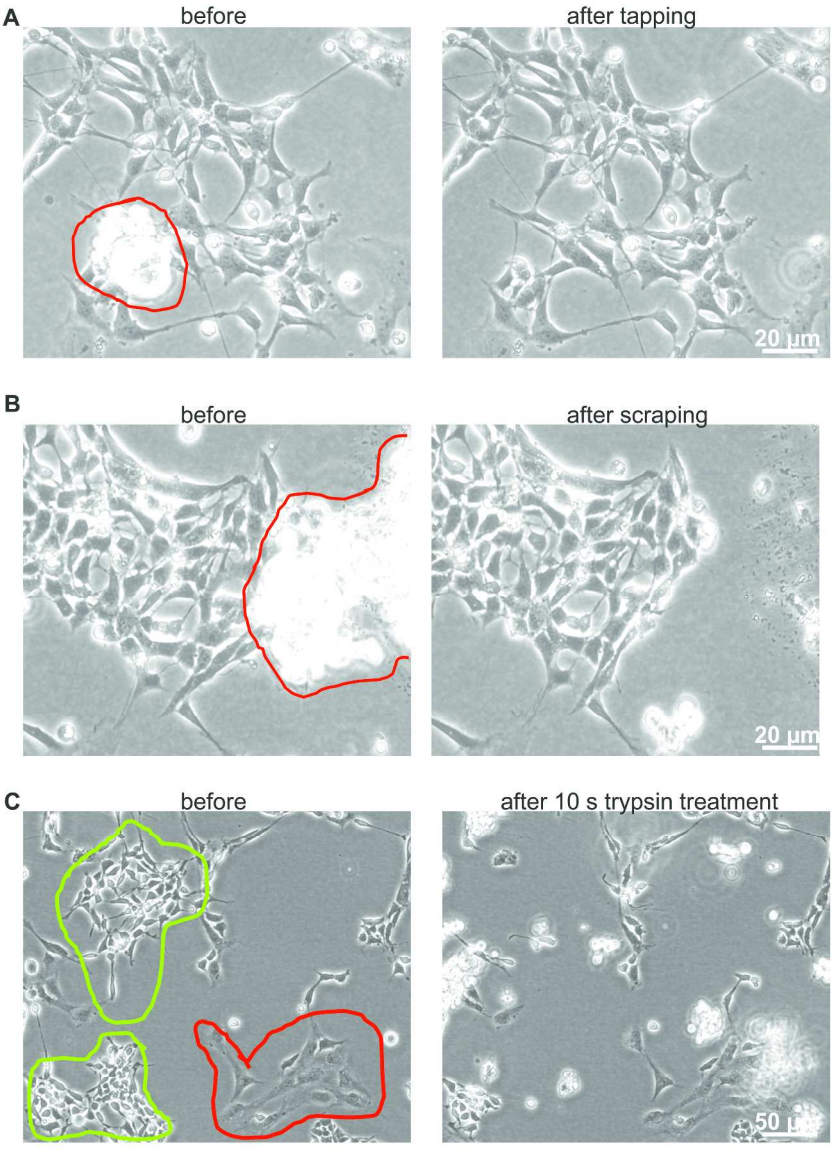

Supplemental figure S2. Kleiderman et al. 2015

217x302mm (600 x 600 DPI)

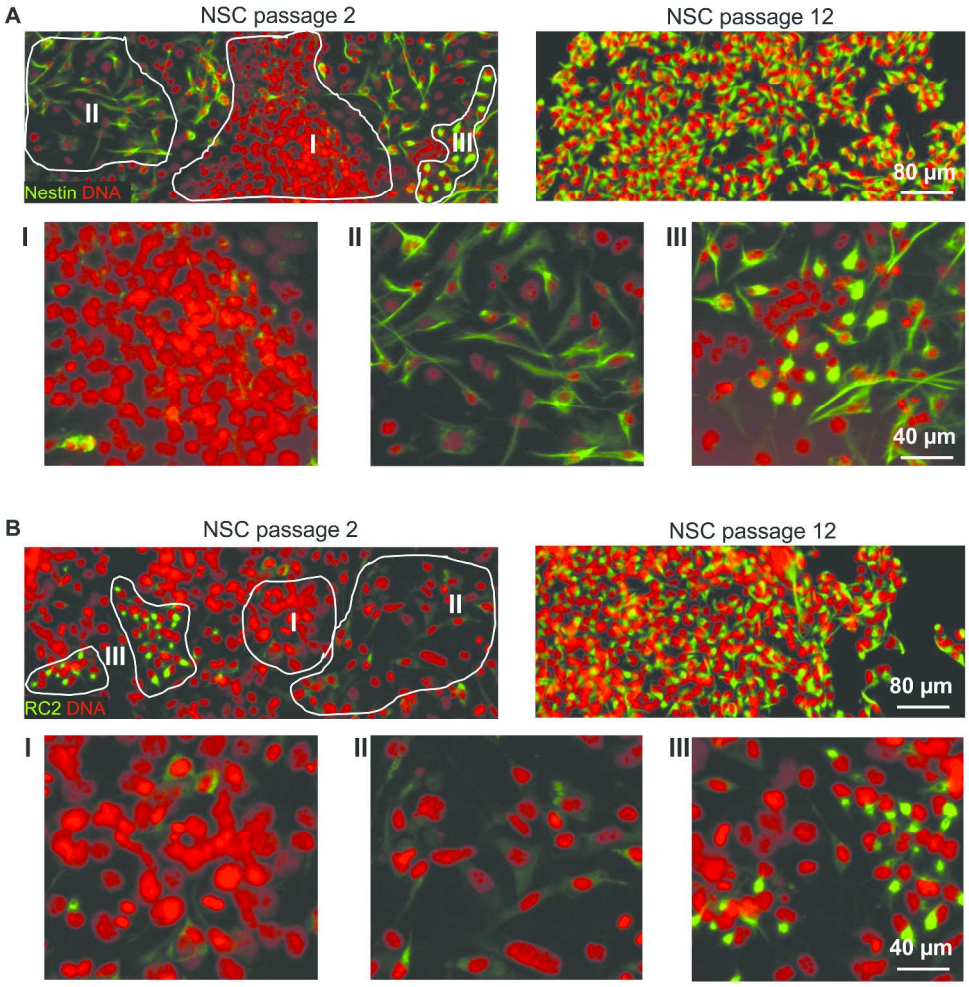

Supplemental figure S3. Kleiderman et al. 2015

203x216mm (600 x 600 DPI)

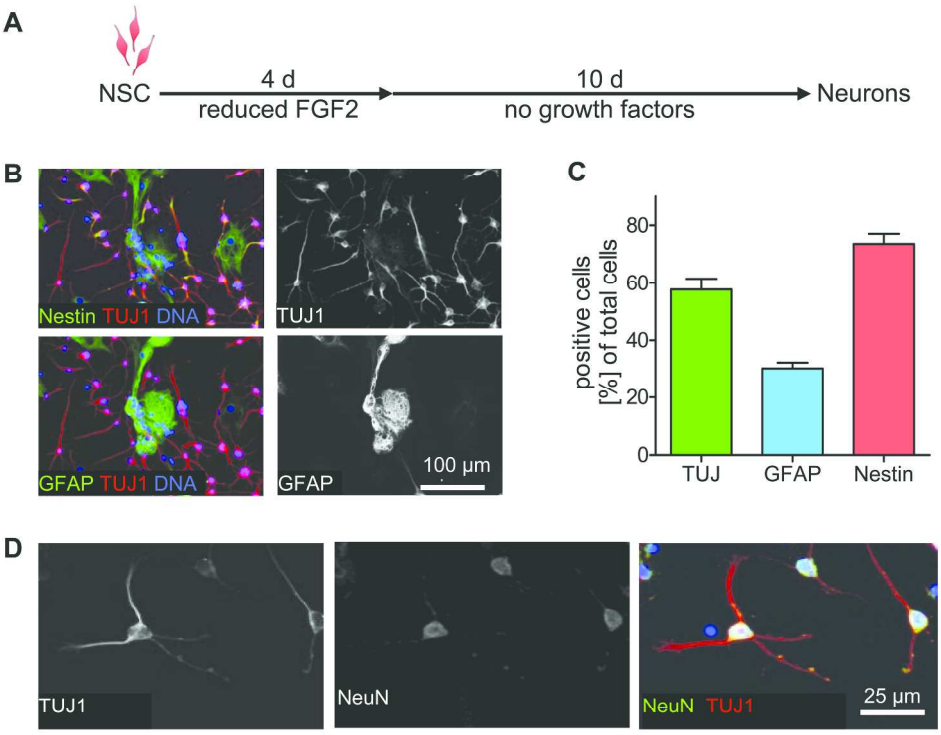

Supplemental figure S4. Kleiderman et al. 2015

132x112mm (600 x 600 DPI)

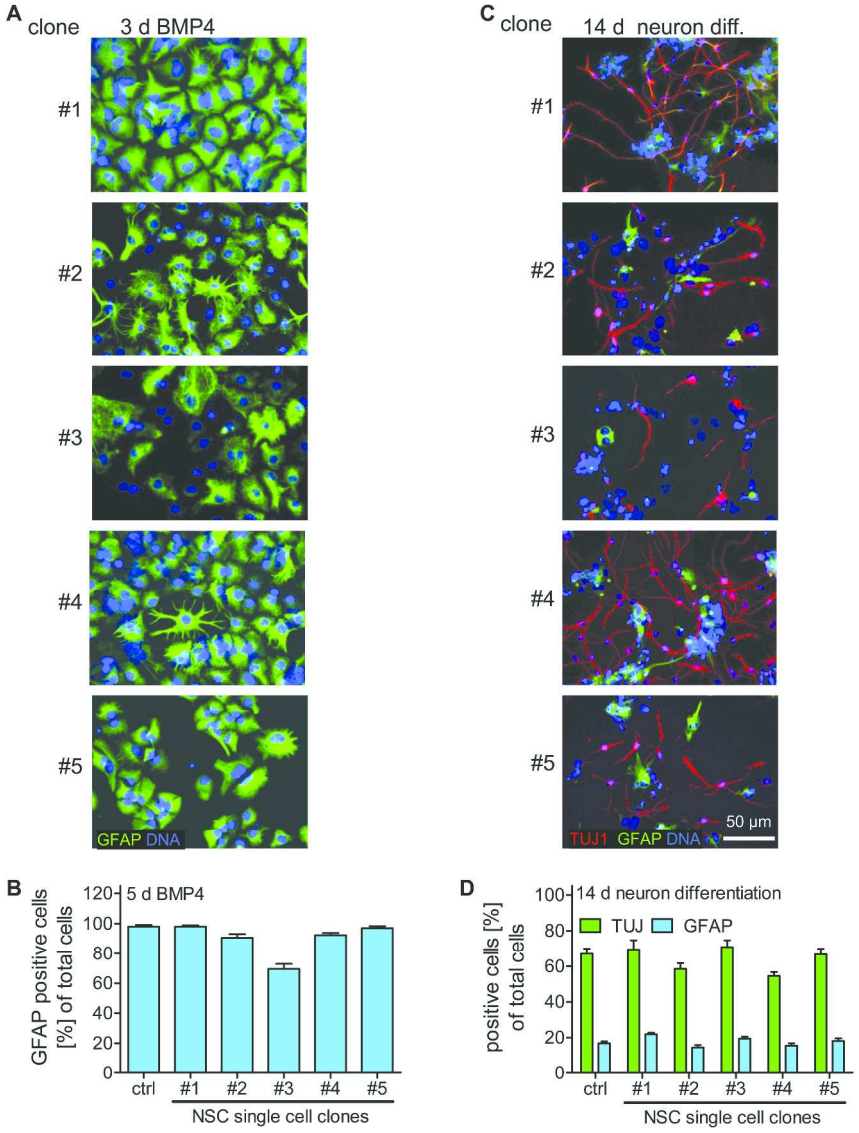

Supplemental figure S5. Kleiderman et al. 2015

233x320mm (600 x 600 DPI)

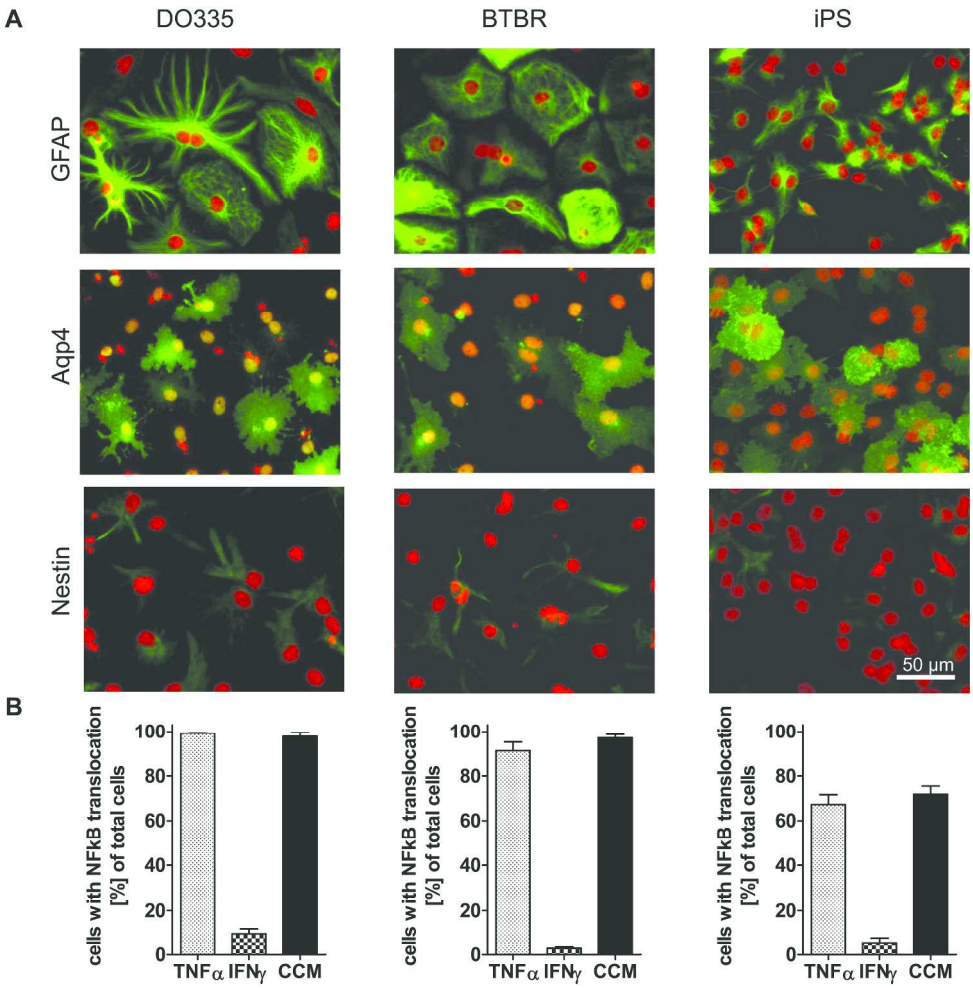

Supplemental figure S6. Kleiderman et al. 2015

180x189mm (600 x 600 DPI)

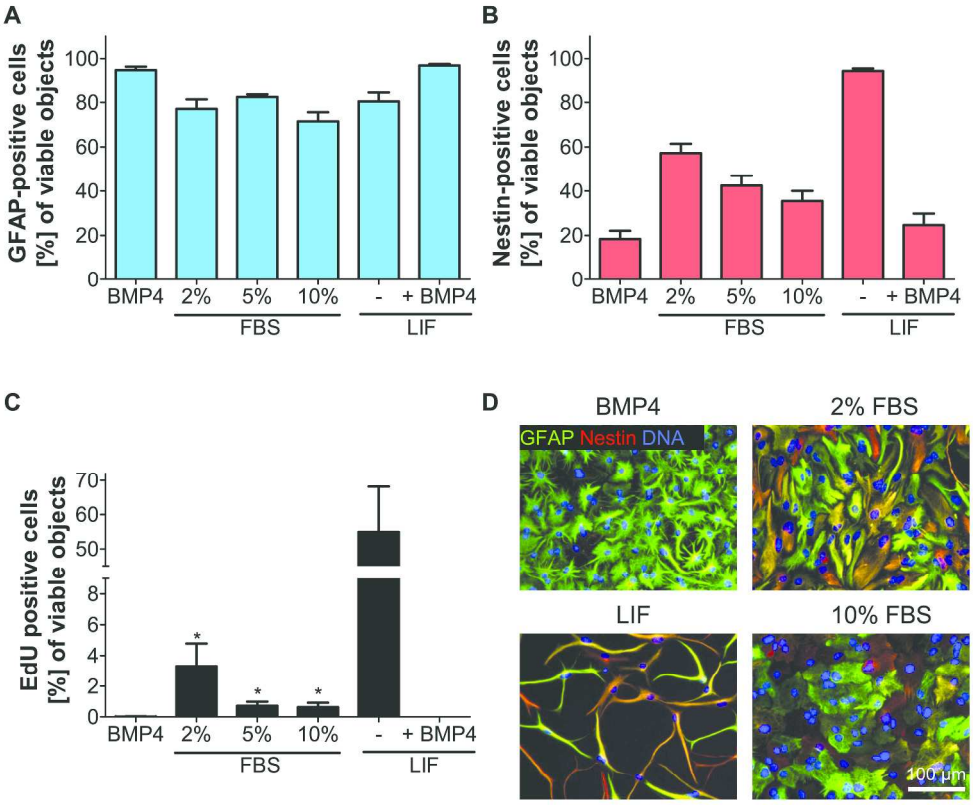

Supplemental figure S7. Kleiderman et al. 2015

157x141mm (600 x 600 DPI)

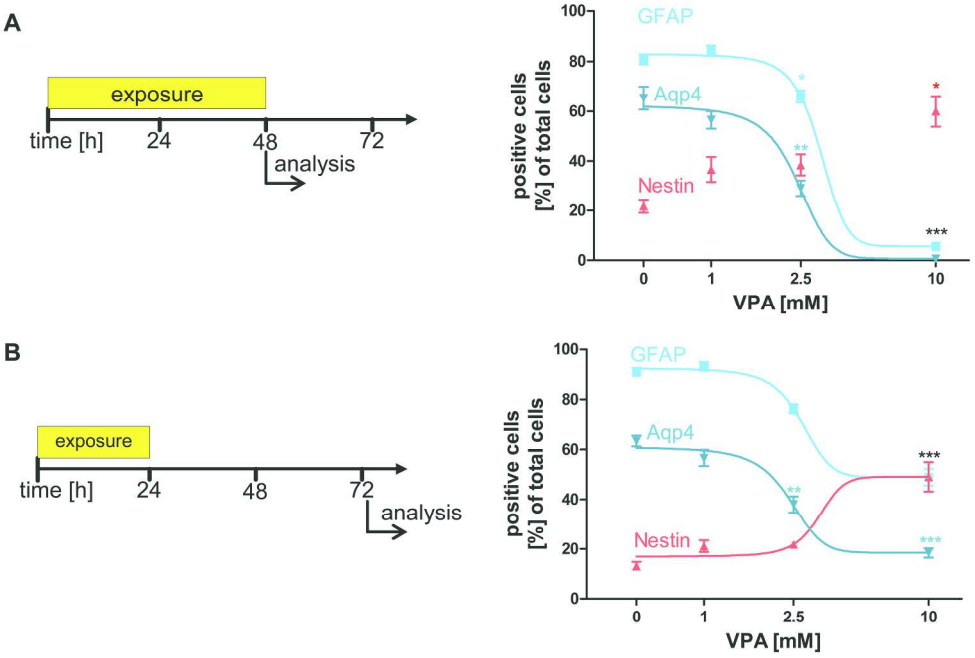

Supplemental figure S8. Kleiderman et al. 2015

128x93mm (600 x 600 DPI)

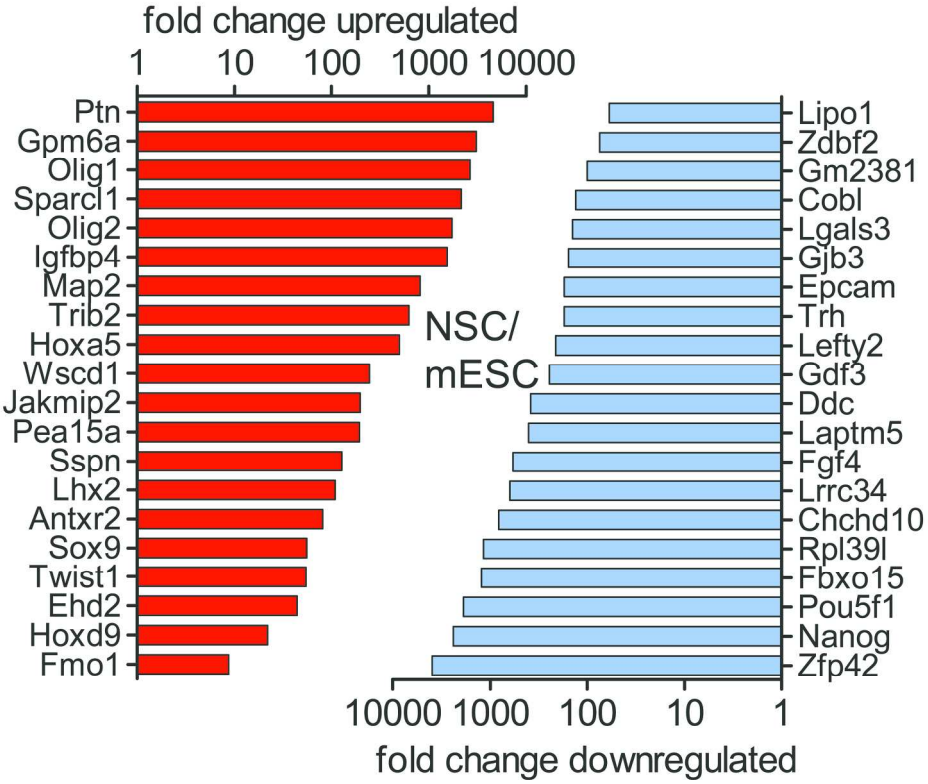

Supplemental figure S9. Kleiderman et al. 2015

106x98mm (600 x 600 DPI)

A Top 20 upregulated genes in mAGES relative to NSC

Name	Affymetrix ID	Full name	log2 (intensity) NSC	log2 (intensity) mAGES	Function
Fmod	1456084_x_at	Fibromodulin	2.7	15.2	Metabolism ECM organization
Aplnr	1438651_a_at	Apelin receptor	2.2	14.2	Development
Cryab	1416455_a_at	Crystallin alpha B	2.5	13.2	Morphogenesis Apoptosis
Cxcr7	1417625_s_at	Chemokine receptor 7	2.4	12.8	Chemotaxis Angiogenesis Cell adhesion
Lyz1	1439426_x_at	Lysozyme 1	2.2	10.0	Metabolism Defence
Nsg2	1416107_at	Neuron specific gene family member 2	6.6	14.4	Vesicle assembly Receptor signaling
Rnf182	1434982_at	Ring finger protein 182	2.7	10.3	Ubiquitination Glutamic acid ligase activity
Col23a1	1440911_at	Collagen type XXIII alpha 1	2.2	9.3	Heparin binding Protein assembly
Gm5817	1435198_at	Predicted gene 5817	2.5	9.4	
Lyz2	1423547_at	Lysozyme 2	2.2	8.9	Metabolism Defence
Timp2	1420924_at	Tissue inhibitor of metallopeptidase 2	2.3	8.3	Proliferation Neuron differentiation
Ndrg4	1426615_s_at	N-myc downregulated gene family member 4	6.1	11.7	Brain development
N4bp2l1	1417707_at	Nedd 4 binding protein 2-like 1	3.1	8.6	Ubiquitination
Id1	1425895_a_at	Inhibitor of DNA binding 1	9.3	14.7	BMP signaling Differentiation Angiogenesis
Peli2	1436966_at	Pellino 2	3.7	8.6	Toll signaling
Id4	1423260_at	Inhibitor of DNA binding 4	2.5	6.7	Proliferation Differentiation Brain development
Arhgef10	1452302_at	Rho guanine nucleotide exchange factor (GEF) 10	2.8	6.5	Mitosis Stress fibre assembly Signal transduction
Letm2	1447987_at	Leucine zipper-EF-hand containing trans-membrane protein 2	2.4	5.3	
Itm2b	1418000_a_at	Integral membrane protein 2B	12.5	14.8	Apoptosis Beta-amyloid binding
Cmtm6	1451114_at	CKLF-like MARVEL trans-membrane domain containing 6	9.0	10.5	Chemotaxis

Supplemental figure S10A. Kleiderman et al. 2015

237x341mm (600 x 600 DPI)

B Top 20 downregulated genes in mAGES relative to NSC

Name	Affymetrix ID	Full name	log2 (intensity) NSC	log2 (intensity) mAGES	Function
Ccnb1	1448205_at	Cyclin B1	12.9	3.4	Cell cycle
Hmmr	1425815_a_at	Hyaluronan-mediated motility receptor	10.8	2.3	Metabolism
Aspm	1422814_at	Abnormal spindle homolog	10.7	2.4	Cell cycle Brain development
Prc1	1423774_a_at	Protein regulator of cytokinesis 1	10.5	2.4	Cytokinesis Cell cycle
Shcbp1	1416299_at	SHC SH2-domain binding protein 1	11.0	2.9	NSC proliferation FGF signaling
Ncapg	1429171_a_at	Non-SMC condensin I complex subunit G	10.3	2.2	Mitosis
Ttk	1449171_at	TTK protein kinase	10.3	2.4	Mitosis
Nek2	1437580_s_at	NIMA (never in mitosis gene a)-related expressed kinase 2	10.0	2.2	Mitosis Cell cycle
Mis18bp1	1434767_at	MIS18 binding protein 1	10.0	2.2	Mitosis
Esco2	1428304_at	Establishment of sister chromatid cohesion N-acetyltransferase 2	9.8	2.3	Cell cycle
Aurka	1424511_at	Aurora kinase A	10.3	2.8	Mitosis Cell cycle
Kif23	1455990_at	Kinesin family member 23	9.8	2.4	Mitosis Cell cycle
Ckap2l	1435938_at	Cytoskeleton associated protein 2-like	9.6	2.3	NSC mitosis
Mcm5	1415945_at	Minichromosome maintenance complex component 5	10.1	2.9	Cell cycle
Ndc80	1417445_at	NDC80 kinetochore complex component	9.7	2.8	Mitosis Cell cycle
Cdc25c	1456077_x_at	Cell division cycle 25C	9.3	2.5	Cell cycle
Nuf2	1430811_a_at	NDC80 kinetochore complex component	8.3	2.2	Mitosis
Wdhd1	1435114_at	WD repeat and HMG-box DNA binding protein 1	8.5	2.5	Chromatin organization
Atad5	1435597_at	ATPase family, AAA domain containing 5	8.4	2.4	DNA damage
Clspn	1441984_at	Claspin	6.7	2.4	DNA damage Cell cycle

Supplemental figure S10B. Kleiderman et al. 2015

220x293mm (600 x 600 DPI)

C Top 20 upregulated genes in mAGES relative to NSC, sorted by fold change

Name	Affymetrix ID	Full name	log2 (intensity) NSC	log2 (intensity) mAGES	Function
Fmod	1456084_x_at	Fibromodulin	2.7	15.2	Metabolism ECM organization
Aplnr	1438651_a_at	Apelin receptor	2.2	14.2	Receptor activity Development
Gfap	1426509_s_at	Glial fibrillary acidic protein	2.2	13.6	Cytoskeletal organization Astrocyte Development
Cryab	1416455_a_at	Crystallin, alpha B	2.5	13.2	Apoptosis Development
Cxcr7	1417625_s_at	Chemokine receptor 7	2.4	12.8	Chemotaxis Angiogenesis Cell adhesion
C3	1423954_at	Complement component 3	2.2	12.7	Immune response Signal transduction
Fbxo2	1427004_at	F-box protein 2	3.6	14.0	Protein modification Differentiation
Hspb8	1417014_at	Heat shock protein 8	2.6	12.6	Protein binding
Mia	1419608_a_at	Melanoma inhibitory activity	2.3	12.0	ECM organization Adhesion
Rnase1	1416523_at	Ribonuclease, RNase A family, 1	2.3	11.9	RNA hydrolysis
Serpinf1	1453724_a_at	Serpin peptidase inhibitor, clade F, member 1	2.8	12.3	Angiogenesis Neurogenesis
Cox8b	1449218_at	Cytochrome c oxidase subunit VIIIb	2.2	11.7	Metabolism
Slc39a12	1436611_at	Solute carrier family 39 member 12	2.3	11.7	Zink ion transport Signal transduction
Cntn1	1459197_at	Contactin 1	2.5	11.6	Adhesion Cerebellum Development
C1qtnf3	1422606_at	C1q and tumor necrosis factor related protein 3	2.2	11.2	Inflammatory response
Myoc	1450468_at	Myocilin	2.2	11.1	Adhesion Migration Differentiation
Aqp4	1425382_a_at	Aquaporin 4	2.2	10.9	Water homeostasis
Lrrc8a	1428394_at	Leucine rich repeat containing 8A	2.7	11.2	Ion homeostasis
Plscr2	1448961_at	Phospholipid scramblase 2	2.2	10.8	Membrane maintenance
Clu	1418626_a_at	Clusterin	2.4	10.8	Apoptosis Proliferation Differentiation

Supplemental figure S10C. Kleiderman et al. 2015

239x339mm (600 x 600 DPI)

D Top 20 downregulated genes in mAGES relative to NSC, sorted by fold change

Name	Affymetrix ID	Full name	log2 intensity NSC	log2 intensity mAGES	Function
Dcpp1	1459725_s_at	demilune cell and parotid protein 1	13.2	2.5	Development
Mki67	1426817_at	marker of proliferation Ki-67	12.5	2.4	Cell cycle
Top2a	1454694_a_at	topoisomerase II alpha	12.9	3.2	DNA binding Cell cycle
Ccnb1	1448205_at	cyclin B1	12.9	3.4	Cell cycle
Ube2c	1452954_at	ubiquitin-conjugating enzyme E2C	12.6	3.3	Ubiquitination Cell cycle
Cep55	1452242_at	centrosomal protein 55	11.7	2.4	Cytokinesis Cell cycle
Bub1	1424046_at	BUB1 mitotic checkpoint serine/ threonine kinase	11.8	2.5	Mitosis Cell cycle
Birc5	1424278_a_at	baculoviral IAP repeat-containing 5	11.8	2.6	Cytokinesis Cell cycle
Pbk	1448627_s_at	PDZ binding kinase	12.1	3.0	Stress response
Nusap1	1416309_at	nucleolar and spindle associated protein 1	11.4	2.4	Mitosis Cell cycle
Ccnb2	1450920_at	cyclin B2	11.3	2.4	Cell cycle
Depdc1a	1424292_at	DEP domain containing 1a	11.0	2.4	Signal transduction
Cenpf	1427161_at	centromere protein F	10.9	2.3	Mitosis Cell cycle
Hells	1417541_at	helicase, lymphoid specific	11.2	2.6	DNA binding Cell cycle
Hmmr	1425815_a_at	hyaluronan-mediated motility receptor (RHAMM)	10.8	2.3	Metabolism
Ect2	1419513_a_at	epithelial cell transforming 2	11.2	2.7	Morphogenesis Apoptosis Cytokinesis
Kif20a	1449207_a_at	kinesin family member 20A	11.0	2.5	Cytokinesis
Grm5	1455272_at	glutamate receptor, metabotropic 5	10.7	2.3	Signal transduction Synaptic transmission
Hmgn5	1418152_at	high-mobility group nucleosome binding domain 5	11.4	3.0	DNA binding Chromatin modification
Prc1	1423774_a_at	Protein regulator of cytokinesis 1	10.5	2.4	Cell cycle

Supplemental figure S10D. Kleiderman et al. 2015

206x254mm (600 x 600 DPI)

E Top 20 upregulated genes in NSC relative to mESC

Name	Affymetrix ID	Full name	log2 (intensity) mESC	log2 (intensity) NSC	Function
Ptn	1448254_at	Pleiotrophin	2.2	14.4	CNS development Cell cycle
Gpm6a	1456741_s_at	Glycoprotein m6a	2.2	13.8	CNS development Differentiation
Olig1	1416149_at	Oligodendrocyte transcription factor 1	2.3	13.6	CNS development Transcription
Sparcl1	1416114_at	SPARC-like 1	2.7	13.8	Signal transduction
Olig2	1416232_at	Oligodendrocyte transcription factor 2	2.2	13.0	CNS development Transcription
Igfbp4	1423756_s_at	Insulin-like growth factor binding protein 4	2.3	12.9	Signal transduction Metabolism Proliferation
Map2	1434194_at	Microtubule-associated protein 2	3.3	12.9	Axonogenesis Cytoskeleton organization
Trib2	1426640_s_at	Tribbles homolog 2	2.7	12.0	Signal transduction Metabolism
Hoxa5	1448926_at	Homeobox A5	2.3	11.2	Anterior/posterior patterning
Wscd1	1455845_at	WSC domain containing 1	2.6	10.6	Metabolism
Jakmip2	1436552_at	Janus kinase and microtubule interacting protein 2	2.3	9.9	Protein binding
Pea15a	1416406_at	Phosphoprotein enriched in astrocytes 15A	2.7	10.3	Signal transduction Apoptosis Transport
Sspn	1417644_at	Sarcospan	2.2	9.2	Cell adhesion
Lhx2	1418317_at	LIM homeobox protein 2	2.2	9.0	CNS development Dorsal/ventral patterning
Antxr2	1426708_at	Anthrax toxin receptor 2	2.2	8.6	Reproduction Toxin transport
Sox9	1424950_at	SRY (sex determining region Y)-box 9	2.4	8.2	Differentiation NSC maintenance
Twist1	1418733_at	Twist basic helix-loop-helix transcription factor 1	2.3	8.0	Differentiation Morphogenesis
Ehd2	1459823_at	EH-domain containing 2	2.3	7.7	Cytoskeleton organization Endocytosis
Hoxd9	1419126_at	Homeobox D9	3.0	7.5	Anterior/posterior patterning Morphogenesis
Fmo1	1417429_at	Flavin containing monooxygenase 1	3.2	6.3	Metabolism

Supplemental figure S10E. Kleiderman et al. 2015

246x368mm (600 x 600 DPI)

F Top 20 downregulated genes in NSC relative to mESC

Name	Affymetrix ID	Full name	log2 (intensity) mESC	log2 (intensity) NSC	Function
Zfp42	1418362_at	Zinc finger protein 42	14.2	2.2	Transcription Embryonic development
Nanog	1429388_at	Nanog homeobox	13.5	2.3	Cell cycle Embryonic development Stem cell maintenance
Pou5f1	1417945_at	POU domain, class 5, transcription factor 1	13.1	2.2	Transcription Cell fate committment Stem cells maintenance
Fbxo15	1427238_at	F-box protein 15	12.5	2.2	Protein binding
Rpl39l	1423327_at	Ribosomal protein L39-like	12.4	2.2	Translation
Chchd10	1433720_s_at	Coiled-coil-helix-coiled-coil-helix domain containing 10	11.9	2.3	Mitochondrion organization Metabolism
Lrrc34	1429366_at	Leucine rich repeat containing 34	11.5	2.2	
Fgf4	1420085_at	Fibroblast growth factor 4	11.4	2.2	Proliferation Apoptosis Differentiation Stem cell maintenance
Laptm5	1436905_x_at	lysosomal-associated protein transmembrane 5	11.0	2.3	Transport
Ddc	1426215_at	Dopa decarboxylase	10.8	2.2	Metabolism Transport
Gdf3	1449288_at	Growth differentiation factor 3	10.2	2.2	Signal transduction Differentiation Cell fate commitment
Lefty2	1436227_at	Left-right determination factor 2	9.9	2.2	Cell growth Development
Trh	1418756_at	Thyrotropin releasing hormone	9.7	2.2	Hormone-mediated signaling
Epcam	1416579_a_at	Epithelial cell adhesion molecule	9.7	2.2	Cell-cell adhesion Proliferation Differentiation
Gjb3	1416715_at	Gap junction protein, beta 3	9.5	2.2	Cell communication Placenta development
Lgals3	1426808_at	Lectin, galactose binding, soluble 3	9.5	2.4	Chemotaxis Migration Proliferation Differentiation
Cobl	1434917_at	Cordon-bleu WH2 repeat	9.3	2.2	Cytoskeleton organization
Gm2381	1443052_at	Predicted gene 2381	8.9	2.2	
Zdbf2	1456783_at	Zinc finger, DBF-type containing 2	8.5	2.2	Nucleic acid binding
Lipo1	1433914_at	Lipase, member O1	8.1	2.2	

Supplemental figure S10F. Kleiderman et al. 2015

233x327mm (600 x 600 DPI)

Mean absolute expression values [log_2] of 94 selected cell type specific genes shown in the heatmap of Fig. 5.

Gene	Accession nr.	mESC	NSC	mAGES
Tfcp2l1	NM_023755	12.49	2.24	2.24
Fbxo15	NM_015798	12.49	2.24	2.24
Dppa2	NM_028615	12.17	2.24	2.24
Tdh	NM_021480	12.84	2.24	2.24
Pou5f1	NM_013633	13.10	2.24	2.24
Fgf4	NM_010202	11.40	2.24	2.24
Esrrb	NM_011934	11.47	2.24	2.32
Dppa4	NM_028610	11.08	2.24	2.24
Zfp42	NM_009556	14.17	2.24	2.24
Lin28a	NM_145833	9.40	2.24	2.24
Gjb3	NM_008126	9.53	2.25	2.31
Eras	NM_181548	9.65	2.24	2.24
Zic3	NM_009575	9.21	2.24	2.24
Tex19.1	NM_028602	10.10	2.24	2.24
Lefty2	NM_177099	9.95	2.24	2.24
Klf4	NM_010637	10.64	2.66	2.53
Nanog	NM_028016	13.55	2.32	3.51
Dppa5a	NM_025274	14.93	3.94	4.92
Tdgf1	NM_011562	13.89	2.24	3.62
Timp1	NM_011593	9.90	5.77	6.38
Msh6	NM_010830	13.34	10.70	7.34
Msh2	NM_008628	11.53	9.00	7.10
Phf17	NM_172303	12.04	7.94	5.69
Lefty1	NM_010094	7.14	2.24	2.24
Utf1	NM_009482	5.76	2.24	2.24
Gab1	NM_021356	11.79	9.08	10.99
Sox2	NM_011443	12.50	12.98	9.42
Cd9	NM_007657	12.07	11.53	12.85
Gnl3	NM_178846	11.97	12.21	7.57
Nes	NM_016701	2.71	10.18	4.59
Sox11	NM_009234	2.24	9.84	8.99
Tcf4	NM_013685	8.81	12.35	11.77
Bmi1	NM_007552	8.97	12.42	9.70
Runx1	NM_001111022	2.29	4.22	3.52
Dcx	NM_010025	2.24	3.58	2.62
Cspg4	NM_139001	2.28	2.58	3.55
Egfr	NM_207655	2.24	10.49	5.25
Lpar4	NM_175271	2.77	5.16	5.33
Meis1	NM_010789	3.74	8.12	8.99
Hes1	NM_008235	8.51	8.43	7.97
Dll3	NM_007866	4.54	4.38	4.01
Ireb2	NM_022655	10.69	9.85	7.39
Nfe2l2	NM_010902	10.86	10.36	11.03
Hes6	NM_019479	6.02	11.91	10.94
Cdh2	NM_007664	2.93	9.96	10.65
Fabp7	NM_021272	2.39	15.11	12.74
Olig2	NM_016967	2.24	12.99	10.50
Pax6	NM_013627	2.40	8.52	9.58
Metrn	NM_133719	2.24	6.09	13.15
Notch1	NM_008714	7.15	10.94	12.53
Ascl1	NM_008553	2.35	8.92	10.62
Rtn1	NM_153457	4.46	11.42	12.82
Pex2	NM_008994	6.39	10.02	10.59
Nr2f1	NM_010151	2.24	11.51	12.94
Wnt5a	NM_009524	2.28	8.85	9.59
Olig1	NM_016968	2.26	13.63	13.45
Nedd9	NM_001111324	3.00	6.69	11.26
Fgfr2	NM_201601	3.04	4.73	6.55

Gene	Accession nr.	mESC	NSC	mAGES
Gfap	NM_001131020	2.25	2.24	13.62
Aqp4	NM_009700	2.24	2.24	10.91
Slc39a12	NM_001012305	2.31	2.32	11.67
Mertk	NM_008587	3.62	3.93	6.93
Cyp4f14	NM_001204336	2.24	2.24	6.57
Pygb	NM_153781	7.32	7.90	13.73
Acta2	NM_007392	5.60	5.96	11.75
Ntsr2	NM_008747	2.24	2.25	7.88
Id2	NM_010496	2.24	2.30	9.25
Fgfr3	NM_001163216	2.24	2.24	10.86
Ccdc80	NM_026439	2.37	7.09	11.87
Agt	NM_007428	8.24	4.18	12.07
Atp1a2	NM_178405	2.51	6.89	8.43
Aldoc	NM_009657	8.45	12.80	15.06
Kcne1l	NM_021487	2.27	6.23	9.91
Pbxip1	NM_146131	5.11	10.06	12.26
Tlcd1	NM_026708	3.60	6.78	7.93
Slc9a3r1	NM_012030	6.88	7.42	9.02
Thrsp	NM_009381	3.30	9.01	11.93
S100b	NM_009115	2.96	9.69	11.32
Nfix	NM_001081982	2.76	11.25	13.45
Slc25a18	NM_001081048	2.25	8.53	10.07
Mlc1	NM_133241	2.82	11.15	13.59
Csad	NM_144942	7.97	9.74	10.23
Sox9	NM_011448	2.39	8.19	9.77
Mgst1	NM_019946	5.19	13.04	14.25
Tnc	NM_011607	2.28	10.96	11.23
Sparcl1	NM_148938	2.74	13.81	14.40
Slc1a3	NM_148938	2.86	10.96	9.81
Acsbg1	NM_053178	2.26	9.87	9.19
Ezr	NM_009510	12.14	10.95	7.40
Numb	NM_001136075	8.47	7.93	9.45
Aldh1L1	NM_027406	6.39	2.78	4.99
Id4	NM_031166	4.71	2.54	10.62
Gja1	NM_010288	10.44	12.00	2.66
Glul	NM_008131	10.65	12.34	12.51

Supplemental figure S11. Kleiderman et al. 2015

233x329mm (600 x 600 DPI)

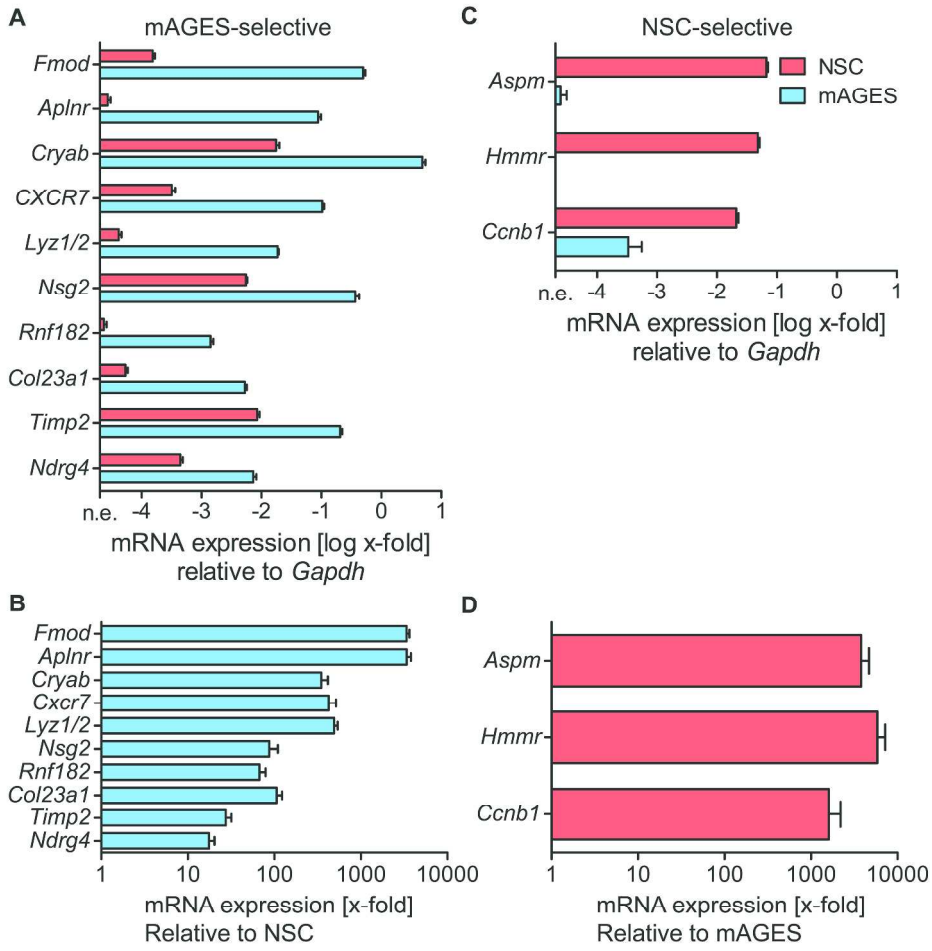

Supplemental figure S12. Kleiderman et al. 2015

180x184mm (600 x 600 DPI)

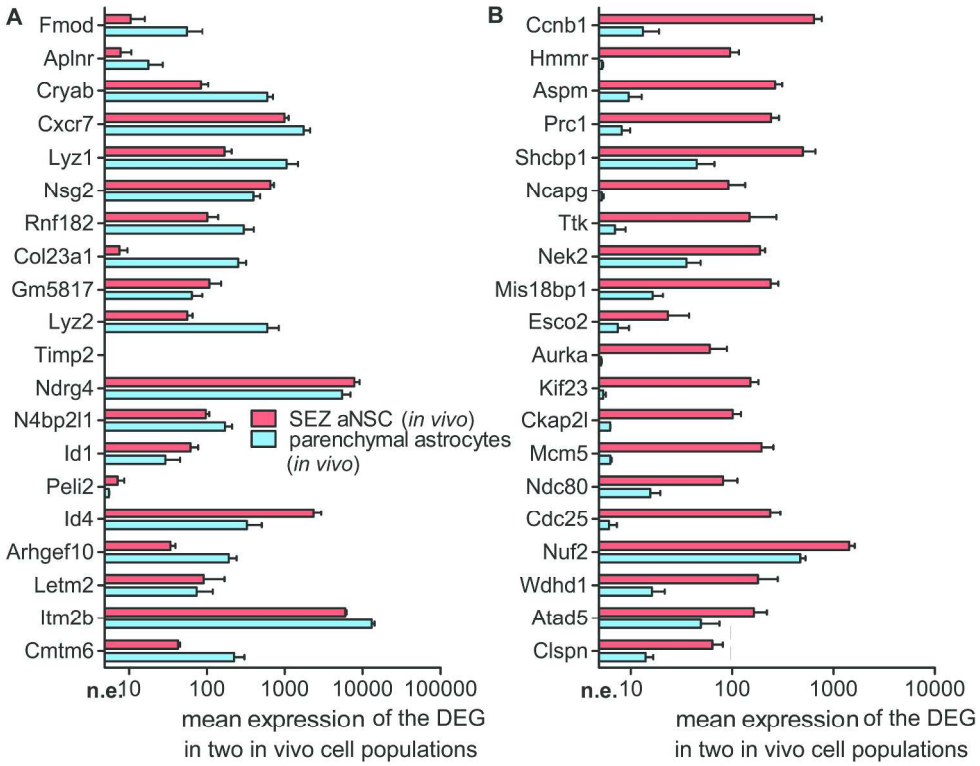

Supplemental figure S13. Kleiderman et al. 2015

159x136mm (600 x 600 DPI)

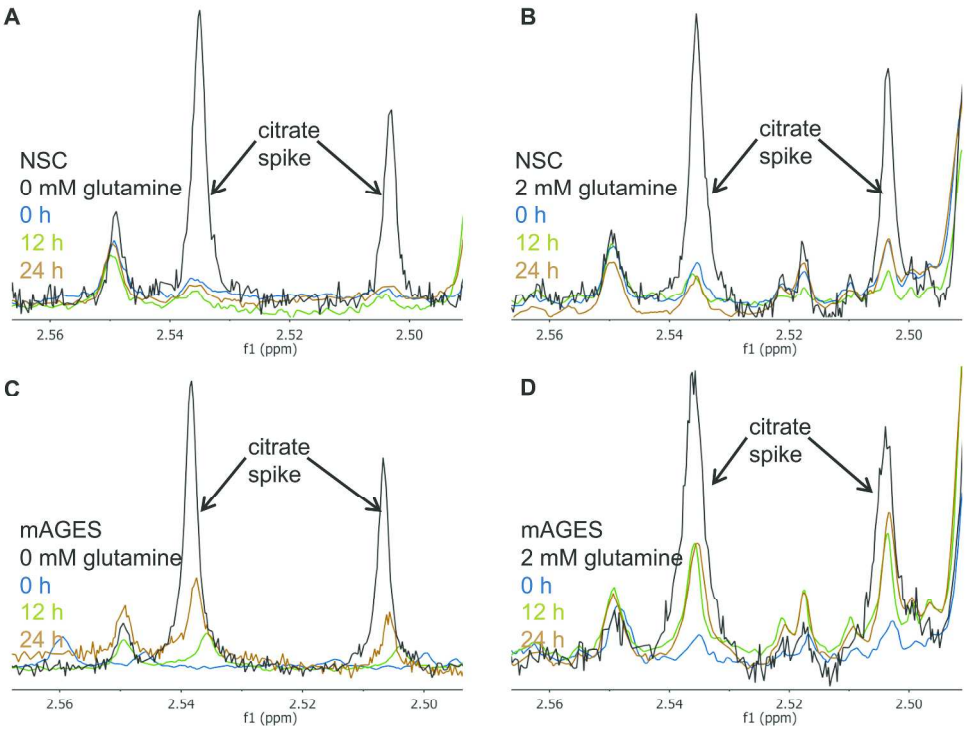

Supplemental figure S14. Kleiderman et al. 2015

150x121mm (600 x 600 DPI)

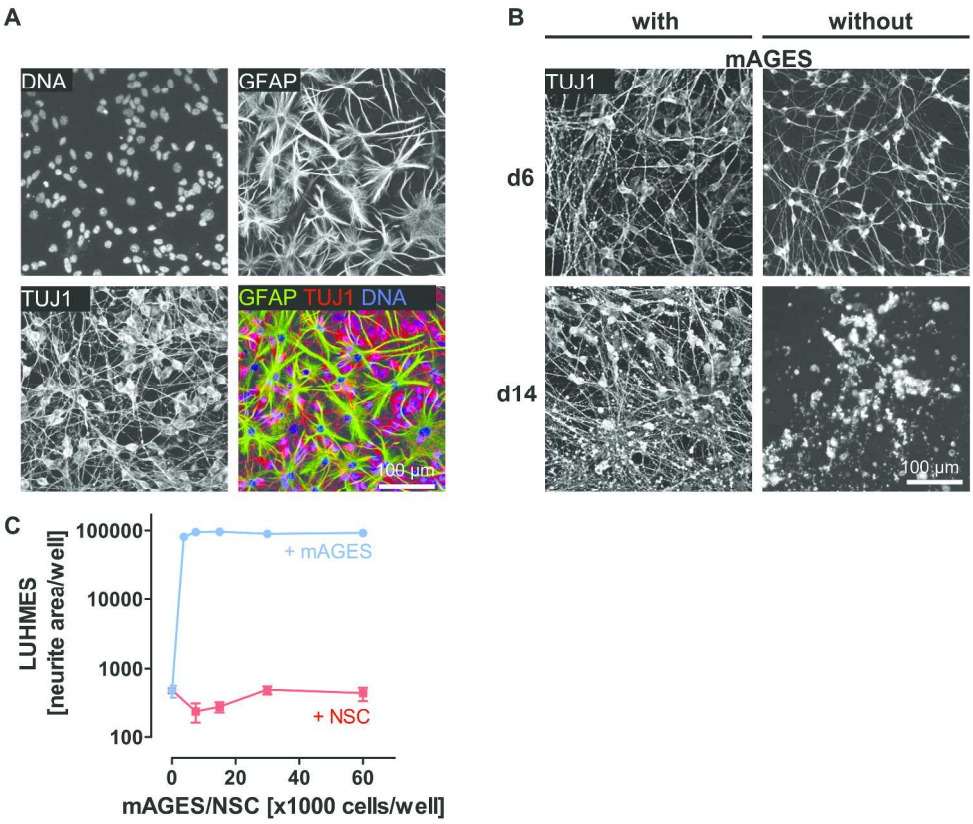

Supplemental figure S15. Kleiderman et al. 2015

161x145mm (600 x 600 DPI)

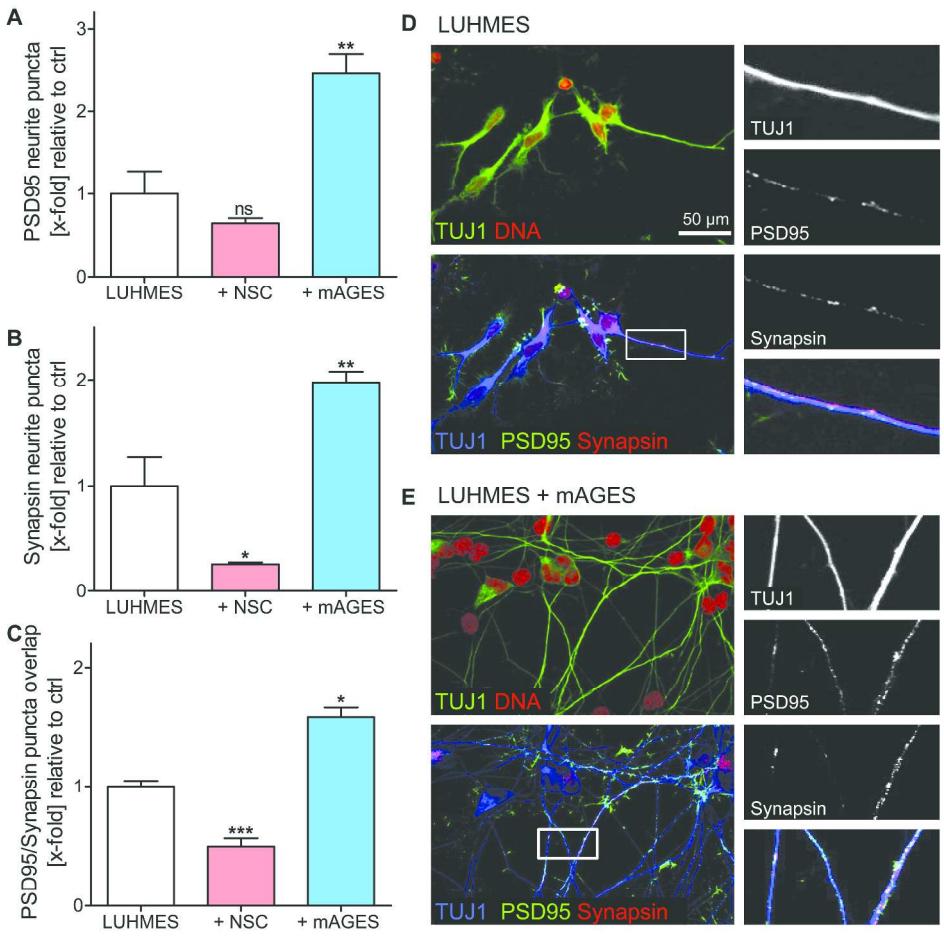

Supplemental figure S16. Kleiderman et al. 2015

191x191mm (600 x 600 DPI)

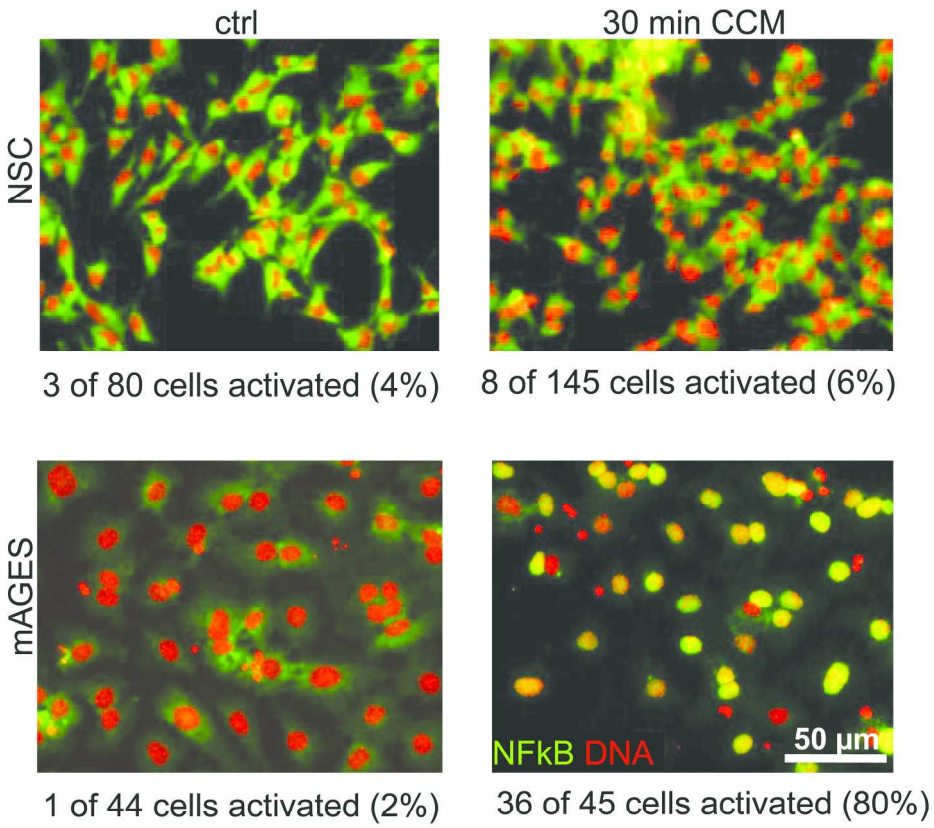

Supplemental figure S17. Kleiderman et al. 2015

117x108mm (600 x 600 DPI)

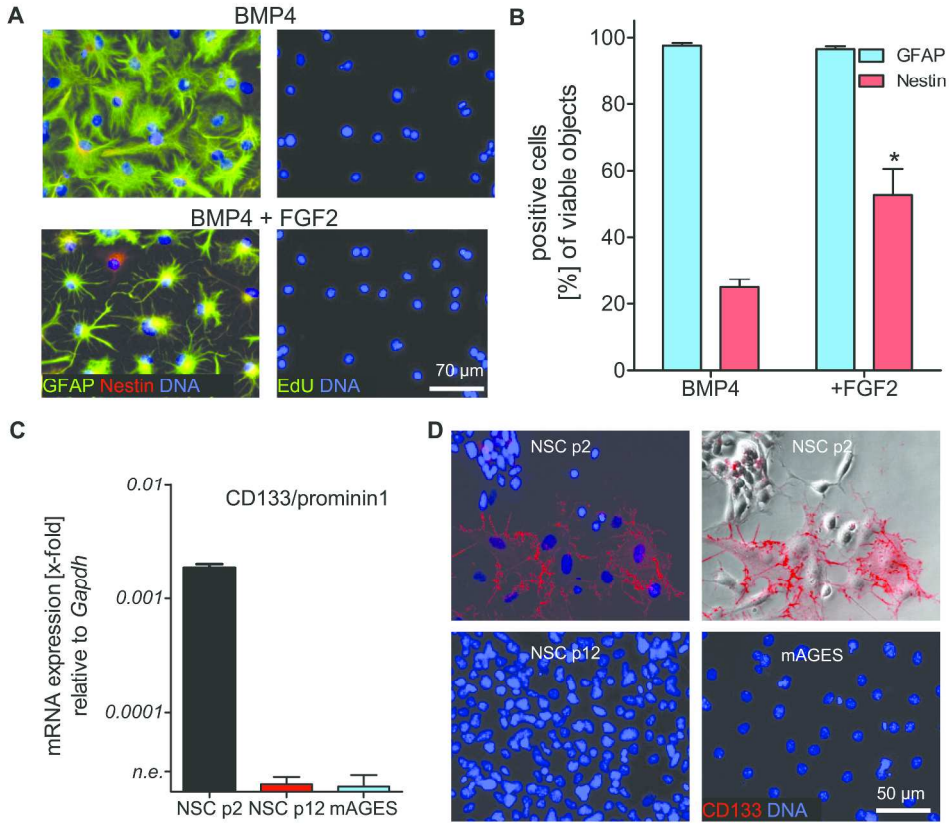

Supplemental figure S18. Kleiderman et al. 2015

166x150mm (600 x 600 DPI)